ZIP9 is a Druggable Determinant of Sex Differences in Melanoma

Cristina Aguirre-Portolés[1], Riley Payne[2], Aspen Trautz[1], J. Kevin Foskett[2], Christopher A. Natale[1], John T. Seykora[1], Todd W. Ridky[1]*

[1]Department of Dermatology, Perelman School of Medicine, University of Pennsylvania.
[2]Department of Physiology, Perelman School of Medicine, University of Pennsylvania, Philadelphia, PA. USA.
*Correspondence to: ridky@pennmedicine.upenn.edu

Abstract

Melanoma and most other cancers occur more frequently, and have worse prognosis, in males compared with females. Though sex steroids are thought to be involved, classical androgen and estrogen receptors are not detectable in most melanomas. Here we show that testosterone promotes melanoma proliferation by activating ZIP9 (*SLC39A9*), a zinc transporter that is not intentionally targeted by available therapeutics, but is widely expressed in human melanoma. This testosterone activity requires zinc influx, MAPK activation and YAP1 nuclear translocation. We demonstrate that FDA approved inhibitors of the classical androgen receptor also inhibit ZIP9, and thereby antagonize the pro-tumorigenic effects of testosterone in melanoma. In male mice, androgen receptor inhibitors suppressed growth of ZIP9-expressing melanomas, but had no effect on isogenic melanomas lacking ZIP9, nor on melanomas in females. These data suggest that ZIP9 might be effectively targeted in melanoma and other cancers by repurposing androgen receptor inhibitors that are currently approved only for prostate cancer.

Introduction

Cancer incidence and mortality are higher in males than in females in the U.S. and worldwide[1,2]. In the U.S., males are 15% more likely to develop cancer, and 40% more likely to die from this disease than females[1]. These sex differences were recognized as early as 1949[3], are observed in the majority of cancer types from non-reproductive tissues[1], and remain even after controlling for known risk factors such as environmental and occupational exposures[4]. While recent advances in modern targeted and immune therapeutics have markedly improved survival for both female and male melanoma patients[5], females still have more favorable outcomes[1,4]. Defining the mechanisms underlying the broad and persistent sex differences in cancer incidence and outcomes will address a major unresolved question in cancer pathobiology.

We previously showed that the female sex hormone estradiol inhibits melanoma proliferation and tumor growth *in vivo*. This effect is independent of biologic sex of the tumor, independent of classical estrogen receptors (ER), and results from activation of a nonclassical surface estrogen receptor on melanocytes and melanoma cells called the G Protein Estrogen Receptor (GPER)[6,7]. This work led us to consider whether male sex hormone signaling might also contribute to female vs. male differences in melanoma progression.

Testosterone is the most abundant androgen and circulates at much higher levels in males (630 ng/dl) than in females (32 ng/dl)[8]. This androgen promotes proliferation *in vitro* in non-gonadal cell types including adipocytes[9], mouse skeletal muscle myoblasts[10], glioblastoma-derived cells[11], lung cancer cell lines[12] and melanoma[13]. As the classical androgen receptor (AR) is not consistently detected in most of these tissues, the receptor(s) mediating the testosterone-dependent increased proliferation and the corresponding downstream mechanisms are not yet

52 defined. Also unknown is whether this androgen activity observed *in vitro* is relevant to cancer
53 progression *in vivo*.
54 Here, we define a nonclassical testosterone signaling pathway that establishes a novel
55 mechanistic link between male androgens and melanoma behavior, and highlights a new
56 therapeutic opportunity using currently-available drugs.
57

58 **Results**
59

60 **Melanoma tumors grow more quickly in male vs. female mice**
61
62 To test whether preclinical melanoma models recapitulate the male vs. female survival disparity
63 observed in humans, we first determined growth of human BRAF-driven melanoma (WM46,
64 female origin, $BRaf^{V600E}$; $CDK4^{R24C}$). Tumors grew faster in immunodeficient SCID male mice
65 compared with matched female mice (Fig. 1A and Fig. S1A), indicating that the differences do
66 not depend on T and/or B cell immune responses. To test whether this phenotype extends to a
67 genetically-engineered preclinical mouse model, we used murine YUMM1.7 cells (male origin,
68 $BRaf^{V600E/wt}$;$Pten^{-/-}$CdkN2a$^{-/-}$)[14] in syngeneic immunocompetent C57BL/6 mice. These tumors
69 also consistently grew faster in male mice compared with matched females (Fig. S1B).
70

71 **Testosterone, but not dihydrotestosterone, promotes proliferation in melanoma cells**
72 **independent of the classical androgen receptor**
73 Physiologic concentrations of testosterone promoted proliferation of both normal early passage
74 primary human melanocytes and melanoma cells (Fig. 1B, C and Fig. S1C). The proliferative
75 response to testosterone correlated to the dose and was saturable, suggesting a specific receptor-
76 mediated activity. In contrast, dihydrotestosterone (DHT) had no effect on proliferation of these

77 cell types across a wide concentration range (Fig. 1C). Dihydrotestosterone is a more potent AR
78 agonist than testosterone[15,16]. The fact that the melanocytes and melanoma cells responded to
79 testosterone, but not to DHT (Fig. 1B, 1C, Fig S1D, E), suggests the possibility that a
80 nonclassical androgen receptor mediates testosterone effects in these cells. Supporting this idea,
81 we were unable to detect AR mRNA transcript in any of the 7 melanoma cell lines (Table S1)
82 and primary melanocyte (MC) cultures we tested, although AR mRNA was readily detectable in
83 prostate cancer cells (Fig. 1D, Fig. S1F). Consistent with this lack of AR transcript, we were also
84 unable to detect AR protein in these cells via western blotting using 2 different AR antibodies, or
85 via immunofluorescence directly on the cultured cells, although AR protein was readily
86 detectable in 2 prostate cancer lines used as positive controls (Fig. 1E and Fig. S1G).

87 To begin testing whether a nonclassical androgen receptor mediates testosterone effects
88 in melanoma we looked to *SLC39A9*/ZIP9, a transmembrane zinc transporter recently discovered
89 in Atlantic Croaker (fish) cells to be a activated by androgen, and unlike AR, to have much
90 higher affinity for testosterone than for dihydroteststerone[17]. ZIP9 transports zinc (Zn^{++}) across
91 cell and organelle membranes into the cytoplasm and is the only steroid receptor known to
92 directly regulate zinc homeostasis[18]. The human ZIP9 homolog, encoded by the *SLC39A9* gene,
93 is broadly expressed in most cancers (Fig. S2A), normal human melanocytes, and all melanoma
94 lines that we tested (Fig. 2A). To test whether ZIP9 was active in melanoma we used the
95 fluorescent Zn^{++}-specific probe FluoZin-3. Testosterone induced a rapid increase in cytosolic
96 free Zn^{++} ($[Zn^{++}]_i$) in human melanoma cells (Fig. 2B), that was followed by a sustained
97 elevation for at least 2 days in the presence f testosterone (Fig. 2C). We determined that Zn^{++}
98 influx was necessary for the testosterone-dependent increase in melanoma cell proliferation, as
99 treatment with the Zn^{++} chelator N,N,N′,N′-tetrakis (2-pyridinylmethyl)-1,2-ethanediamine

100 (TPEN), blocked testosterone induced proliferation at TPEN concentrations that had no
101 significant effect on proliferation when used alone (Fig. 2D and Fig. S2B).

102 Although TPEN has high affinity for Zn^{++}, it also has some ability to chelate copper[19]. To
103 test whether copper flux might contribute to testosterone effects on melanoma proliferation, we
104 treated WM46 cells with $CuSO_4$, which had no significant effect on cell proliferation (Fig. S2C).
105 Moreover, the highly specific copper chelator bathocuproinedisulfonic acid (BCS), did not affect
106 the proliferative response to testosterone, nor did BCS affect testosterone induced Zn^{++} influx
107 (Fig. S2D and Fig. S2E).

108 After determining that Zn^{++} influx was necessary for testosterone-induced proliferation,
109 we next tested whether increased Zn^{++} was sufficient to increase melanoma proliferation.
110 Exogenous zinc pyrithione (also a Zn^{++} ionophore), and $ZnCl_2$ each increased melanoma
111 proliferation (Fig. 2E). Other biologically-relevant divalent cations, Fe^{++} and Mn^{++}, known to be
112 transported by other ZIP family members[20], had no effect on proliferation (Fig. 2E). Together,
113 these results demonstrate that testosterone, but not DHT, promotes zinc dependent proliferation
114 in melanoma cells that express ZIP9 and lack detectable AR.

115 We next used immunocytochemistry to test whether AR and/or ZIP9 protein are
116 expressed in human melanocytic lesions (14 benign nevi, 63 primary melanomas, and 21
117 metastatic melanomas). AR was determined in tissue sections using a highly validated CLIA
118 (Clinical Laboratory Improvement Amendments) certified method in the clinical pathology lab at
119 the Hospital of the University of Pennsylvania. This procedure uses a validated antibody
120 different from the two we used for western blotting and immunofluorescence. Each tissue was
121 scored in a blinded fashion by a board-certified pathologist. While AR was readily detectable in
122 prostate tissue used as positive control, AR was not detected in any of the nevi, nor in the

123 melanomas (Fig. 2F). In parallel, we analyzed the same samples for ZIP9. CLIA grade ZIP9
124 IHC is not available. However, we validated our ZIP9 antibody using parental WM46 ZIP9
125 positive (wtZIP9) and isogenic ZIP9 negative (ΔZIP9) cell lines. These cells were grown on
126 chamber slides and processed for IHC in parallel with the human samples. The antibody used
127 labeled only the wtZIP9 cells. ZIP9 protein was observed in 100% of the nevi, 97% of primary
128 melanomas and 100% of the metastatic samples (Fig. 2G). Further, ZIP9 relative staining
129 intensity positively correlated with tumor stage (Fig. 2H). No significant differences in ZIP9
130 staining were observed between males and females (Fig. S3).
131
132 **Testosterone signaling through ZIP9 promotes melanoma growth**
133 To determine whether ZIP9 mediates testosterone effects in our models, we used CRISPR-Cas9
134 and gRNA targeting Slc39A9 exon1 to ablate ZIP9 in human (WM46) melanoma and in murine
135 (YUMM1.7) melanoma. Isogenic clonal populations of parental ZIP9-expressing (wtZIP9) and
136 ZIP9-ablated (ΔZIP9) cells were established, and the mutations disrupting the reading frame
137 were mapped by sequencing (Fig. S4A, S4B and S4C). ZIP9 protein was not detectable in ΔZIP9
138 cells (Fig. 2F, Fig. 3A, Fig. 3B and Fig. S4D). ΔZIP9 cells did not respond to testosterone,
139 whereas isogenic wtZIP9 control clones responded similarly to the parental wtZIP9 cells (Fig.
140 3A, 3B and Fig. S4E).
141 The testosterone insensitive phenotype associated with CRISPR-Cas9 engineered ZIP9 loss
142 was rescued by expression of a human ZIP9 transgene. Lentiviral mediated constitutive ZIP9
143 expression in the ΔZIP9 WM46 cells restored both ZIP9 protein and the proliferative response to
144 testosterone, verifying the on target effects of the CRISPR-Cas9 mediated ZIP9 ablation (Fig.
145 S4F, S4G).

146 Consistent with the conclusion that ZIP9 is the major mediator of testosterone and
147 exogenous zinc effects in these melanoma cells, exposure to testosterone or to extracellular zinc
148 failed to increase $[Zn^{++}]_i$ in ΔZIP9 cells (Fig. 3C and 3D). Therefore, testosterone induces a
149 rapid, ZIP9-dependent, increase in $[Zn^{++}]_i$ that is required for the increased proliferation in
150 melanoma cells.
151

152 **Testosterone-induced melanoma proliferation through ZIP9 requires downstream MAPK**
153 **and YAP1 activation**

154 Although the studies detailed above show that testosterone promotes melanoma proliferation via
155 ZIP9 dependent Zn^{++} influx, zinc is involved in myriad cellular processes, making it difficult to
156 predict *a priori* which downstream signaling pathways are required for the testosterone activity.
157 To start identifying these, we used a 447-element Reverse Phase Protein Array (RPPA) analysis
158 of human WM46 melanoma cells treated with testosterone for 0, 30, 60 and 480 min. While the
159 relative expression of most represented proteins was unaffected by testosterone, some were
160 significantly under or overexpressed, including several with known tumor-promoting or tumor-
161 suppressive functions (Fig. 4A and Table S2). Downregulated proteins included 14-3-3ε, a tumor
162 suppressor and negative YAP1 regulator previously implicated in liver, lung, and gastric
163 cancers[21], and CDKN2A (p16), a cyclin-dependent kinase (CDK) inhibitor, and one of the most
164 studied tumor suppressors[22]. Upregulated proteins included key elements of tumor-promoting
165 pathways, most notably phosphorylated ERK (T202; Y204) and YAP1 (Fig. 4A).
166 Importantly, ΔZIP9 cells displayed decreased basal levels of ERK phosphorylation compared
167 with isogenic wild-type clones (Fig. S5A). MAPK activation was necessary for the testosterone-
168 dependent proliferative response, as the specific ATP-competitive ERK1/2 inhibitor, ulixertinib[23]

169 (RVD-523; Ei) blocked the testosterone-dependent proliferative response, at ulixertinib
170 concentrations that had no effect on the basal proliferation rate when used alone (Fig. 4B).
171 Testosterone-dependent ZIP9 activation appeared to render WM46 cells more sensitive to
172 ulixertinib, as cell viability was compromised when they were treated with both testosterone and
173 RVD-523. This vulnerability to combination treatment seems to be specific and ZIP9 dependent,
174 as ΔZIP9 cells treated with both testosterone and ulixertinib proliferated at rates comparable to
175 controls (Fig. 4B).

176 We determined that YAP1 activation is also required for the augmented proliferative
177 response driven by testosterone. YAP1 is a transcriptional coactivator whose activity is largely
178 regulated by its localization[24]. Testosterone induced rapid YAP1 translocation from cytoplasm to
179 nucleus in human melanoma cells in a ZIP9-dependent manner (Fig. 4C, 4D and Fig. S5B).
180 YAP1 subcellular localization is controlled largely by LATS, which phosphorylates YAP1 at
181 Serine 127 and thereby retains YAP1 in the cytoplasm[25]. The YAP1 inhibitor dobutamine also
182 promotes phosphorylation of YAP at Ser127[26]. Consistent with this, the testosterone induced
183 YAP1 nuclear localization and increase in cell proliferation were both blocked by dobutamine,
184 while this compound had no significant effect on its own (Fig. 4D, Fig. S5C and Fig. 4E). When
185 ZIP9 expression was rescued via lentiviral transduction of a ZIP9 transgene to ΔZIP9 WM46
186 cells, testosterone dependent YAP1 translocation into the nucleus was also restored (Fig. S5C).

187 Testosterone promotion of YAP1 activity was evidenced by increased expression of
188 several well-known YAP1 target genes including CDC6, CTGF, CYR61 and THBS1. As
189 expected, these testosterone-induced expression changes were also blocked by dobutamine (Fig.
190 4F).

191 **Pharmacologic ZIP9 blockade inhibits testosterone-driven melanoma proliferation and**
192 **melanoma tumor growth *in vivo.***

193 We next tested whether FDA-approved compounds could be repurposed to effectively
194 target ZIP9. Although specific ZIP9 inhibitors are not yet developed, molecular modeling and
195 competition assays with fluorescent-tagged testosterone suggest that the androgen receptor
196 inhibitor bicalutamide (BIC) competes with testosterone for ZIP9 binding to the same
197 extracellular pocket and thereby acts as a competitive ZIP9 antagonist[27]. Bicalutamide was
198 developed and approved for prostate cancer and has now been largely replaced by enzalutamide
199 (ENZ) and apalutamide (APA), which are structurally related analogs with higher affinity for the
200 androgen receptor and greater clinical efficacy against advanced prostate cancer[28,29].

201 While ZIP9 was not known to be an androgen receptor at the time these drugs were
202 developed, we show here that they are nonetheless effective inhibitors of testosterone effects in
203 melanoma cells that express ZIP9, but lack detectable AR. Each compound completely blocked
204 testosterone-induced proliferation and MAPK activation in several melanoma cell lines (Fig. 5A,
205 5B). Importantly, these agents alone (without testosterone) had no effect on cell proliferation
206 (Fig. S6A). The testosterone dependent increase of intracellular zinc was also efficiently blocked
207 by bicalutamide (Fig. S6B). Moreover, ΔZIP9 cells transduced to re-express ZIP9, responded to
208 testosterone, and this effect was again blocked by bicalutamide (Fig. S6C).

209 To further confirm that these pharmacologic agents work through ZIP9, we next used
210 cyproterone acetate (CPA), an anti-androgen that blocks the testosterone interaction with AR, but
211 that does not bind to ZIP9[30]. In our melanoma cells, up to a 20-fold molar excess of CPA did not
212 significantly inhibit testosterone effects on proliferation, consistent with the conclusion that AR
213 is not the major mediator of testosterone effects in these melanoma models (Fig. S6D).

214 To test whether these pharmacologic flutamide class AR inhibitors block the physical
215 interaction between testosterone and ZIP9 in melanoma, we performed direct binding assays
216 using a membrane-impermeable testosterone analogue (T-BSA-FITC). This reagent labels the
217 plasma membrane surface of wild-type ZIP9 expressing WM46 melanoma cells (Fig. 5C). This
218 membrane bound testosterone was displaced by apalutamide, demonstrating the specificity of the
219 interaction (Fig. 5C). Further demonstrating that the binding is ZIP9 specific, testosterone
220 localization at the plasma membrane was markedly reduced in ΔZIP9 cells (Fig. 5C) that did not
221 respond to either testosterone, or to APA in vitro (Fig. 5D).
222 Next, we tested whether apalutamide and related analogs inhibit melanoma *in vivo*. For this, we
223 introduced wtZIP9 or isogenic ΔZIP9 human WM46 melanoma into SCID mice. Once-daily
224 systemically administered apalutamide (20 mg/kg/day via oral gavage) significantly suppressed
225 growth of wtZIP9 tumors in male mice and extended its survival (doubling time for tumor
226 growth was 11.1 days for vehicle treated males and 25.2 days for APA treated males) (Fig. 5E,
227 Fig. S7A). Similar results were obtained when males were treated with bicalutamide
228 (30mg/kg/day) (Fig. S7B). Importantly, bicalutamide had no effect on wtZIP9 tumors in female
229 mice, nor on ΔZIP9 tumors (Fig. S7C and S7C). Together, these data show that ZIP9 promotes
230 melanoma progression specifically in males.
231

232 **Discussion**

233
234 Although many have speculated that sex steroids contribute to sex differences in cancer
235 pathobiology, definitive functional studies are lacking, and the mechanisms by which they
236 contribute to the male-female cancer sex gap are largely unknown. We previously described the
237 tumor suppressor activity of the nonclassical estrogen receptor GPER in melanoma[6]. This

238 finding led us to question whether circulating androgens in males might also contribute to the
239 melanoma sex gap.

240 Testosterone promoted proliferation of melanoma cells in a saturable-dose-dependent
241 manner. Curiously, the same cell lines did not respond to DHT, which is generally considered
242 the more biologically active androgen. DHT displays 4-fold increased affinity than testosterone
243 for AR, and it dissociates from AR three time slower than testosterone[16]. Lack of response to
244 DHT in melanoma is consistent with the absence of detectable AR expression in the models used
245 for this study, and is highly consistent with our genetic data showing that ZIP9, which has higher
246 affinity for testosterone vs. DHT, is an important mediator of testosterone effects.

247 We show that ZIP9 activation via testosterone binding promotes an increase in cytosolic
248 zinc in melanoma cells. The mammalian family of zinc transporters SLC39A comprises 14
249 members (ZIP1–14)[31] grouped into four subfamilies that were stablished according to their
250 amino acid sequence similarities. There may be roles for these other family members in some
251 cancers, as ZIP1 (SLC39A1, from ZIPII subfamily) that has been associated with the regulation
252 of zinc uptake in prostate cancer cells[32]. However, this rapid increase of intracellular zinc
253 through ZIP1 appears to be AR dependent, as PC-3 cells only respond to testosterone after they
254 are transfected with exogenous AR. ZIP9 amino acid residues predicted to be most critical for
255 testosterone and bicalutamide binding include Ala167, Val241, Met248, and Ala167, Leu302,
256 Ser171, respectively[27], however only Ala167 is present in ZIP1, suggesting that this receptor
257 may not be similarly regulated by testosterone. Regarding other members of the SLC39A family,
258 ZIP9 is unique member of ZIPI subfamily[33], and the only one known to directly interact with
259 testosterone.

260 A recent report[34] also considered a possible role for testosterone in melanoma and
261 concluded that the androgen promotes melanoma. Authors attributed this effect to the classical
262 AR. However, that report did not consider ZIP9, did not show that AR was necessary for
263 melanoma response to pharmacologic AR inhibitors, and did not show that AR was a
264 determinant of sex differences in melanoma tumor growth. Here we studied 98 human
265 melanocytic lesions (nevus, primary and metastatic melanoma) and did not detect AR in any of
266 them, while ZIP9 protein was detectable in 97% and 100% of the primary and metastatic
267 melanomas respectively. We recognize the possibility that some melanoma cell lines and perhaps
268 even some human tumors, may express AR that also contributes to melanoma growth.

269 There may be many drivers of the cancer sex gap in humans, including differences in
270 immune surveillance[35]. However, differences in immune surveillance do not appear to be a major
271 driver of the differences in the melanoma models used for this study, as tumors progressed faster
272 not only in male vs. female immunocompetent mice, but also in human melanomas grown in
273 male vs. female SCID mice. Therefore, the testosterone effects on melanoma in these models are
274 dependent on ZIP9, but independent of B and T cell mediated anti-tumor activity. Consistent
275 with this, ZIP9 expressing tumors respond to bicalutamide and apalutamide in SCID mice.

276 As ZIP9 is widely expressed in nearly all tissues, it may be a major determinant of the
277 sex disparity in outcomes not just for melanoma, but also for many other cancer types.
278 Consistent with this, we observed that testosterone promotes proliferation in many diverse cancer
279 cell types, and that this effect is blocked by bicalutamide (Fig. S8).

280 The demonstration here that ZIP9 is pharmacologically accessible, suggests that ZIP9
281 may be a new eminently druggable therapeutic target (Fig. 5F), and that currently approved
282 androgen receptor inhibitors might be useful alone, or in combination with current standard of

283 care therapeutics for a wide range of cancers, especially those that disproportionately affect
284 males.
285

286 **Materials and Methods**
287

288 **CRISPR-Cas9 mediated ablation of Slc39A9**

289 We used lentiviral transduction to deliver dox-inducible Cas9 and gRNA targeting exon 1 of
290 Slc39A9 in human WM46 and murine YUMM1.7 melanoma cells. Transduced cells were
291 selected with puromycin, and single cells subsequently isolated, expanded and examined for
292 ZIP9 protein expression, compared to clones isolated in parallel with no doxycycline treatment.
293 The following gRNA sequences were used (5'-3'):
294 hZIP9_gRNA_Fw caccgTTGGTGGGATGTTACGTGGC
295 hZIP9_gRNA_Rv aaacGCCACGTAACATCCCACCAAC
296 hZIP9_gRNA_Fw caccgCGTGGCCGGAATCATTCC
297 hZIP9_gRNA_Rv aaacGGAATGATTCCGGCCACG
298 To map the targeted sequencing, the region surrounding the gRNA target sequence was
299 amplified in both WM46 (282bp) and YUMM1.7 (259bp) isogenic clones. The following
300 primers were used (5'-3'): hZIP9_CRISPRmut_Fw:
301 TAAGCAGAATTCATGGATGATTTCATCTCC
302 hZIP9_CRISPRmut_Rv:TAAGTAAGTCCAAGCTTCTGCTGCTTTGTCTGATGCA.
303 mZIP9_CRISPRmut_F:TAAGCAGAATTCATGGATGACTTTCTCTC.
304 mZIP9_CRISPRmut_Rv TAAGTAAGTCCAAGCTTGATATTTCTGCTGCTTTGT.

305 Once amplified, DNA fragments were cloned into pUC19 vector using EcoRI and HindDIII
306 sites, and sequenced (Sanger) by the DNA Sequencing Facility (University of Pennsylvania).
307 Sequences were analyzed using the free software CRISP-ID (V1.1) and ICE Analysis by
308 Synthego were the knock-out scores were obtained.
309
310 **Cell culture and proliferation assays**
311 YUMM1.7, SH-4 and SK-MEL-2 cells were purchased from ATCC (YUMM1.7 ATCC® CRL-
312 3362™; SH-4 ATCC® CRL-7724™; SK-MEL-2 ATCC® HTB-68™) and cultured in DMEM
313 (Mediatech, Manassas, VA, USA) with 5% FBS (Invitrogen, Carlsbad, CA, USA) and 1%
314 Penicillin-Streptomycin (Thermo Fisher Scientific. # 15140122). SK-MEL-3 cells were
315 purchased from ATCC (ATCC® HTB-69™ and cultured in McCoy's 5A (Modified) Medium
316 with 10% FBS (Invitrogen, Carlsbad, CA, USA) and 1% Penicillin-Streptomycin. SK-MEL-24
317 cells were purchased from ATCC (ATCC® HTB-71™) and cultured in Eagle's Minimum
318 Essential Medium with 15% FBS and 1% Penicillin-Streptomycin. WM46 melanoma cells were
319 a gift from Meenhard Herlyn (Wistar Institute, Philadelphia, PA, USA) and were cultured in
320 TU2% media. Tumor cells were regularly tested using MycoAlert Mycoplasma Detection Kit
321 from Lonza (Allendale, NJ, USA). For monitoring cell proliferation $10x10^5$ YUMM1.7 or
322 $12x10^5$ WM46 cells were seed per well in 12-well Cell culture Plates. All the experiments
323 performed in this work utilized charcoal stripped serum (Fetal Bovine Serum, charcoal stripped,
324 USDA-approved regions, One Shot™ format. Catalogue number #A3382101; Thermofisher
325 Scientific). Cells were treated every second day and manually counted in triplicate using a
326 hemocytometer. All the experiments were performed in cell populations that were in culture
327 during a maximum of 3 weeks (5 passages in average) since thaw from the corresponding stock.

328 **Zinc influx analysis**

329 WM46 cells were loaded with 5 µM FluoZin™-3, AM cell permeant™ (Thermo Fisher
330 Scientific, #F24195), for 20 minutes then incubated in 2 Ca Tyrode's solution (in mM: 140
331 NaCl, 5 KCl, 1 $MgCl_2$, 2 $CaCl_2$, 10 glucose and 5 (Na) Pyruvate – pH 7.4) for 5-10 minutes at
332 room temperature prior to imaging. Cells were imaged on a Nikon Ti microscope using a
333 20x/0.75 NA objective for fluorescence at 340 nm and 380nm excitation/515 nm emission (Ca^{2+}-
334 free Fura2 or FluoZin™-3) and 380 nm excitation/515 nm emission (Ca^{2+}-free Fura2 FluoZin™-
335 3). Coverslips were perfused at 1-3 mL/min following this protocol: Ca^{2+} Tyrode's (0-30 secs);
336 Ca^{2+} Tyrode's + DMSO & 5 uM Zinc (30-90 secs); Ca^{2+} Tyrode's + Testosterone & 5□M Zinc
337 (90-360 secs); Ca^{2+} Tyrode's + Testosterone + BIC & 5 uM Zn (360-470 secs); Ca^{2+} Tyrode's
338 washout (470-500 secs). 100 milliseconds exposure images for each wavelength were collected
339 every 2 seconds. For analyzing the long-term consequences of testosterone treatment, cells were
340 treated with the androgen for 96 hours and then loaded FluoZin™-3. Cells were incubated with
341 FluoZin™-3 following manufacturer recommendation and exposed to 400nM Zn pyrithione or
342 $ZnCl_2$. Images were acquired with EVOS BLA. Fluorescence was quantitated using ImageJ
343 (National Institutes of Health, Bethesda, MD, USA), and statistical analyses were performed
344 using Graphpad Prism software.

345

346 **Reverse Phase Protein Array (RPPA)**

347 We used the Functional Proteomics Core at MD Anderson
348 (https://www.mdanderson.org/research/research-resources/core-facilities/functional-proteomics-
349 rppa-core.html) to perform a 447-element Reverse Phase Protein Array (RPPA) analysis of
350 human melanoma cells grown in medium with stripped serum and treated with testosterone

351 (100nM) for 0, 30', 60' and 8 hours. Cells were tripsinized and washed with PBS. After
352 centrifugation (5 minutes; 1200rpm), supernatant was discarded, and cells were frozen at -80ºC
353 prior to be sent to the Functional Proteomics Core at MD Anderson.
354
355 **Western blot, immunofluorescence and antibodies**
356 Adherent cells were washed once with PBS and lysed with 8M urea containing 50mM NaCl and
357 50mM Tris-HCl, pH 8.3, 10mM dithiothreitol, 50mM iodoacetamide. Lysates were quantified
358 (Bradford assay), normalized, reduced, and resolved by SDS gel electrophoresis on 4–15%
359 Tris/Glycine gels (Bio-Rad, Hercules, CA, USA). Resolved protein was transferred to PVDF
360 membranes (Millipore, Billerica, MA, USA) using a Semi-Dry Transfer Cell (Bio-Rad), blocked
361 in 5% BSA in TBS-T and probed with primary antibodies recognizing β-actin (Cell Signaling
362 Technology, #3700. 1:4000, Danvers, MA, USA), ZIP9 (Abcam, #137205, 1:500), P-ERK (Cell
363 Signaling Technology, Phospho-p44/42 MAPK (Erk1/2) (Thr202/Tyr204) (D13.14.4E) XP®
364 Rabbit mAb #4370. 1:1000), ERK (Cell Signaling Technology, p44/42 MAPK (Erk1/2) (137F5)
365 Rabbit mAb #4695, 1:1000), Androgen Receptor [(D6F11) XP® Rabbit mAb #5153] and
366 Recombinant Anti-Androgen Receptor antibody [EPR1535(2)] (ab133273. Antibody already
367 validated by the Human Protein Atlas). After incubation with the appropriate secondary antibody
368 [(Rabbit Anti-Mouse IgG H&L (Biotin) preabsoFS9rbed (ab7074); Anti-mouse IgG, HRP-linked
369 Antibody #7076. 1:2000)] proteins were detected using ClarityTM Western ECL Substrate (Bio-
370 Rad. #170-5060). All western blots were repeated at least 3 times. To monitor YAP1 nuclear
371 translocation by western blot analysis, nuclear fractionation was performed using protein lysis
372 buffer containing 10mM HEPES, 1mM KCl, 1.5mM MgCl2 and 10% glycerol (Buffer A). After
373 washing the adherent cells with DPBS, samples were resuspended in Buffer A and incubated for

374 5 minutes on ice in the presence of 0.1% Triton-X-100. After centrifugation, the nuclear fraction
375 remained as a pellet while the supernatant corresponding to the cytosolic fraction. Nuclear
376 fraction was washed with Buffer A. After centrifugation, the nuclear fraction was resuspended in
377 RIPA buffer and samples were boiled for 5 min prior to sample loading. The cytosolic fraction
378 was centrifuged for 15 min at 13500 rpm. Only the supernatant was kept after centrifugation.
379 Western blot was performed as described before and the following antibodies were used for
380 protein detection: β-tubulin (Cell Signaling Technology, β-Tubulin (9F3) Rabbit mAb #2128.
381 1:1000), PARP (Cell Signaling Technology, Rabbit mAb #9542. 1:1000), YAP1 (Cell Signaling
382 Technology, YAP (D8H1X) XP® Rabbit mAb #14074. 1:1000). For immunofluorescence in
383 adherent cells, samples were fixed with 4% paraformaldehyde (Affymetrix; #19943) for 7 min at
384 room temperature and permeabilized with iced-cold methanol. After blocking with 10%
385 FBS:0.03%Triton-X100, primary antibodies were incubated overnight in blocking solution (β-
386 actin and YAP1 antibodies detailed above). After three washes in DPBS:0.03% Triton X-100)
387 cells were incubated with secondary antibodies for 45 minutes at room temperature [(Goat anti-
388 Mouse IgG (H+L) Highly Cross-Adsorbed Secondary Antibody, Alexa Fluor 594. Goat anti-
389 Rabbit IgG (H+L) Highly Cross-Adsorbed Secondary Antibody, Alexa Fluor 488)]. Cells were
390 rinsed with PBS-0.03%-Triton three times and coverslips were mounted with ProLong Gold
391 antifade reagent with DAPI (#P36935; Thermo Fisher Scientific). Images were captured using a
392 Leica DM IL microscope and registered using LAS software. For fluorescence intensity
393 quantification ImageJ software (National Institutes of Health, Bethesda, MD, USA) was used,
394 and statistical analyses were performed with GraphPad Prism software.
395
396

397 **Immunohistochemistry and quantification**

398 FFPE tissue microarrays (ME1004h: Malignant melanoma, metastatic malignant melanoma and
399 nevus tissue array) were obtained from US Biomax, Inc. (Derwood, MD). For the staining with
400 anti-ZIP9 antibody [(SLC39A9 Antibody (PA5-52485), Thermofisher Scientific, Waltham,
401 MA)], slides were deparaffinized and rehydrated following the standard immunohistochemistry
402 protocol [(xylenes 5 minutes x 3, 100% alcohol (5 min. x 3), 95% alcohol (5 min.), 80% alcohol
403 (5 min.), 70% alcohol (5 min.), and 50% alcohol (5 min.) and finished with distilled water)]. The
404 antigen retrieval was done by loading the slides into a retriever (Electron Microscopy Sciences
405 EMS) with R-Buffer A. After 20 minutes, samples were allowed to cool for 30 minutes inside
406 the retriever and for 20 minutes at room temperature. Samples were washed twice with PBS and
407 blocked with Dako Dual Endogenous Enzyme Block (Code S2003. Agilent Santa Clara, CA) for
408 20 minutes at R.T. Samples were washed twice with PBS and blocked for 20 minutes with 2
409 drops of Vector Avidin Block. After washing twice with PBS, slides were blocked for 20
410 minutes with two drops of Vector Biotin Block (Avidin/Biotin Blocking kit. SP-2001. Vector
411 Laboratories, Inc. Burlingame, CA). Samples were washed twice with PBS with Protein Block
412 Serum-Free Ready-To-Use for 30 minutes at R.T. (Code X0909. Agilent Santa Clara, CA).
413 Primary antibody was prepared 1:500 in PBST (100µl per slide) and samples were incubated
414 overnight at 4°C. Samples were washed three times with PBS and incubated with Biotinylated
415 Secondary antibody (Vectastain Kit, Peroxidase Rabbit IgG, PK-4001) for one hour at R.T. After
416 three washes with PBS, ABC reagent (prepared 30 minutes in advance) was added and samples
417 were incubated for 30 minutes at R.T. Samples were washed twice with PBS and incubated for 3
418 minutes with ImmPACT® DAB Substrate, Peroxidase (HRP) (SK-4105. Vector laboratories,
419 Burlingame, CA). Tissues were counterstained with hematoxylin (30 seconds, R.T.) (GHS316.

420 Sigma-Aldrich) dehydrated, and mounted with SecureMount (Fisher HealthCare™
421 PROTOCOL™ Mounting Media. #022-208. Fisher Scientific. Thermofisher Scientific). John T.
422 Seykora M.D., Ph.D, performed scoring of the stained tissue microarray, and scoring index was
423 determined by scoring the percentage of positive cells on a scale of 0 to 3 as well as the intensity
424 of ZIP9 staining on a scale of 0 to 4 (1=1-25%, 2=26-50%, 3=51-75%, 4=76-100%).

425 The staining of the tissue microarrays (ME1004h) for AR detection was performed by
426 University of Pennsylvania Pathology Clinical Service Center—Anatomic Pathology Division,
427 using the highest grade, CLIA (Clinical Laboratory Improvement Amendments) certified and
428 validated test available. Briefly, five-micron sections of formalin-fixed paraffin-embedded tissue
429 were stained using antibody against Androgen Receptor [(Leica AR-318-L-CE, clone AR27
430 (clone AR27, 1:25)]. Staining was done on a Leica Bond-IIITM instrument using the Bond
431 Polymer Refine Detection System (Leica Microsystems DS9800). Heat-induced epitope retrieval
432 was done for 20 minutes with ER2 solution (Leica Microsystems AR9640). All the experiment
433 was done at room temperature. Slides are washed three times between each step with bond wash
434 buffer or water. The slides were reviewed and scored in blinded fashion by a board-certified U.
435 Penn pathologist. Prostate tissue was used as the positive control.

436

437 **Immunocytochemistry**

438 To detect ZIP9 protein in WM46 isogenic clones, the protocol described in ProSciΨ™ for
439 immunocytochemistry. Briefly, cells were fixed in 4% PFA for 7 minutes. After two washes with
440 PBS (5min), cells were permeabilized with PBS/0.1% Triton X-100 for 1 minute at R.T. Cells
441 were washed twice with PBS on a shaker. Once treated with 1.5% H_2O_2/PBS solution for 15
442 minutes (R.T.), cells were washed again and blocked with 5%BSA for one hour at R.T. For

443 primary antibody incubation, α-ZIP9 antibody [(SLC39A9 Antibody (PA5-52485),
444 Thermofisher Scientific, Waltham, MA)] was diluted 1:500 in 1% BSA and cells were incubated
445 overnight at 4ºC. After washing three times with PBS on a shaker, the slide was incubated with
446 Biotinylated Secondary antibody (Vectastain Kit, Peroxidase Rabbit IgG, PK-4001) for one hour
447 at R.T. Cells were washed three times with PBS, ABC reagent (prepared 30 minutes in advance)
448 was added and samples were incubated for 30 minutes at R.T. After three washes with PBS,
449 samples were incubated for 1.5 minutes with Vector Laboratories DAB Peroxidase (HRP)
450 Substrate Kit (NC9276270. Vector laboratories, Burlingame, CA). Cells were counterstain with
451 hematoxylin (10 seconds, R.T.) (GHS316. Sigma-Aldrich) and mounted with SecureMount
452 (Fisher HealthCare™ PROTOCOL™ Mounting Media. #022-208. Fisher Scientific.
453 Thermofisher Scientific).
454
455 **Cell membrane labeling with testosterone-BSA-FITC**
456 WM46 were seeded over coverslips in p12-well culture plate, after 24 hours cells TU2% media
457 was removed, and cells were grown in Serum-free TU media for 24 hours. Cells were treated
458 with APA (8mM) or DMSO as vehicle control. After one hour, cells were treated with 0.25μM
459 testosterone 3-(O-carboxymethyl) oxime:BSA-fluorescein isothiocyanate (T-BSA-FITC)
460 conjugate (T5771, Sigma-Aldrich, Munich, Germany) diluted in Tris-Buffer (pH 7.2) for 20 min
461 at room temperature. Negative control cells were incubated with 0.25 μM BSA-FITC (A9771,
462 Sigma-Aldrich, Munich, Germany) diluted in Tris-Buffer (pH 7.2) for 20 min at room
463 temperature. The medium was then aspirated, and cells were fixed for 7 minutes with 4%PFA.
464 Cells were washed three times with PBS (5 minutes each) and mounted with ProLong Gold

465 antifade reagent with DAPI (#P36935; Thermo Fisher Scientific). Images were captured using a
466 Leica DM IL microscope and registered using LAS software.
467
468 **Quantitative RT-PCR**
469 RNA was extracted using RNeasy kit (Qiagen. #74104) following the manufacturer's
470 instructions. cDNA was obtained using High Capacity cDNA Reverse Transcription Kit
471 (Applied Biosystems #4368814). For quantitative real-time PCR, PowerUP™ SYBR™ Green
472 Master Mix (Applied Biosystems #A25741) was used. ViiA 7 Real-Time PCR System was used
473 to perform the reaction (Applied Biosystems). Values were corrected by β-actin expression. The
474 $2^{-\Delta\Delta Ct}$ method was applied to calculate the relative gene expression. Primers used for the
475 amplification are included in Table S2.
476
477 **Mice, subcutaneous tumors and pharmacologic treatments**
478 All mice were purchased from Taconic Biosciences, Inc. (Rensselaer, NY, USA). 8- to 10-week
479 old male and female C57BL/6NTac or IcrTac:ICR-Prkdcscid mice were allowed to reach
480 sexually mature ages or to acclimatize for one week prior to being used in experiments. These
481 studies were performed without inclusion/exclusion criteria or blinding but included
482 randomization. Based on a two-fold anticipated effect, we performed experiments with at least 5
483 biological replicates. All procedures were performed in accordance with International Animal
484 Care and Use Committee (IACUC)-approved protocols at the University of Pennsylvania.
485 Subcutaneous tumors were initiated by injecting tumor cells in 50% Matrigel (Corning, Bedford,
486 MA, USA) into the subcutaneous space on the right flanks of mice. 10×10^6 human WM46 or 10
487 x 10^5 murine YUMM1.7 cells were used for each tumor. Oral administration of vehicle,

488 bicalutamide (30mg/kg/day) or apalutamide (20mg/kg/day) was performed daily. 100µl of drug
489 was administrated by oral gavage [10%DMSO:90%Vehicle (15% ethanol:85% sesame oil)].
490 Weight and health status of the mice as well as tumor growth were monitored daily. As
491 subcutaneous tumors grew in mice, perpendicular tumor diameters were measured using calipers.
492 Volume was calculated using the formula $L \times W^2 \times 0.52$, where L is the longest dimension and
493 W is the perpendicular dimension. Animals were euthanized when tumors exceeded a protocol-
494 specified size of 15 mm in the longest dimension. Secondary endpoints include severe ulceration,
495 death, and any other condition that falls within the IACUC guidelines for Rodent Tumor and
496 Cancer Models at the University of Pennsylvania.
497
498 **Statistical analysis**
499 For experiments comparing two groups (treated vs control), significance was calculated using the
500 Mann-Whitney test. For experiments with more than two groups, one-way ANOVA with
501 Tukey's honest significance difference test was performed. For the tumor growth studies *in vivo*,
502 non-linear regression analysis was performed to get the Exponential Growth Equation and
503 doubling times for tumor growth. To analyze the slopes of the curves and to compare them
504 between groups, linear regression analysis was performed. All the statistical analyses in this
505 work were performed using Graphpad Prism Software. Error bars represent standard error of the
506 mean (SEM). **** p value≤0.0001; *** p value≤0.001; ** p value≤0.01; * p value≤0.05;
507 n.s>0.05.
508
509
510

Acknowledgements

The authors thank the University of Pennsylvania Skin Biology and Disease Research-based center for analysis of tissue sections and University of Pennsylvania Pathology Clinical Service Center—Anatomic Pathology Division for the AR staining of the tissue microarray. **Funding:** T.W.R. is supported by grant from the NIH/NCI (R01 CA163566, R41CA228695), and by the Stiefel award from the Dermatology Foundation. This work was also supported in part by the Penn Skin Biology and Diseases Resource-based Center (P30-AR069589), the Melanoma Research Foundation to T.W.R., and R37 GM56328 to J.K.F**.**

Author Contributions

C.A.P., R.P., A.T. performed the experiments. C.A.P., R.P. and J.K.F designed and performed the experiments to study zinc influx. J.K.F provided experimental material and reviewed the manuscript. J.T.S, scored the tissue microarray and reviewed the manuscript. C.A.P, C.A.N. and T.W.R designed experiments and wrote the article. **Competing interests:** C.A.P., C.A.N., and T.W.R., and are inventors on a provisional patent held by the University of Pennsylvania related to this work.

Conflict of interest

T.W.R., C.A.N and C.A.P. are inventors on a provisional patent held by the University of Pennsylvania related to this work.

534 **<u>The Paper Explained</u>**

535 **The Problem:** Melanoma incidence and mortality are higher in males than females. This sex
536 difference remains, even after controlling for known melanoma risk factors such as
537 environmental and occupational exposures. While modern immune and targeted therapeutics
538 have markedly improved outcomes for many melanoma patients, most with metastatic tumors
539 still die from their disease. There is acute need for identification of new therapeutic targets, and
540 effective agents to safely engage them.

541 **Results:** Here, we define a nonclassical testosterone signaling pathway that establishes a novel
542 mechanistic link between male androgens and melanoma pathobiology. Using medically relevant
543 preclinical in vivo models, we first demonstrate that melanomas progress more rapidly in males
544 vs. females. We then show that 97% of primary melanomas and 100% of metastatic lesions from
545 people express the nonclassical membrane androgen receptor and zinc transporter, ZIP9, and that
546 ZIP9 activation promotes melanoma proliferation. Using complementary pharmacologic and
547 genetic approaches, we show that ZIP9 is a major determinant of the sex dependent difference in
548 tumor growth in vivo, and that ZIP9 may be an eminently druggable new therapeutic target for
549 melanoma.

550 **Impact:** ZIP9 is a zinc transporter that is not intentionally targeted by any available therapeutics
551 but is widely expressed in nearly all tissues. The demonstration that this receptor is
552 pharmacologically accessible suggests that inhibiting ZIP9 by repurposing currently approved
553 inhibitors designed to target the classical androgen receptor (AR) may be useful alone or in
554 combination with current standard of care therapeutics for a wide range of cancers, especially
555 those that disproportionately affect males.

556
557

558 **References**

559

560 1. Siegel, R. L., Miller, K. D. & Jemal, A. Cancer statistics, 2020. *CA Cancer J Clin* **70**, 7–
561 30 (2020).
562 2. GLOBOCAN2018. https://bit.ly/2Vd3C6a.
563 3. Clemmesen, J. & Busk, T. Cancer Mortality Among Males and Females in Denmark,
564 England, and Switzerland: V. Incidence of Accessible and Inaccessible Cancers in Danish Towns
565 and Rural Areas. *Cancer Res* **9**, 415–421 (1949).
566 4. Hieken, T. J. *et al.* Sex-Based Differences in Melanoma Survival in a Contemporary
567 Patient Cohort. *Journal of Women's Health* (2020) doi:10.1089/jwh.2019.7851.
568 5. GLOBOCAN2018. Sex disparities in melanoma survival over time. shorturl.at/bkAI6.
569 6. Natale, C. A. *et al.* Activation of G protein-coupled estrogen receptor signaling inhibits
570 melanoma and improves response to immune checkpoint blockade. *Elife* **7**, (2018).
571 7. Natale, C. A. *et al.* Sex steroids regulate skin pigmentation through nonclassical
572 membrane-bound receptors. *Elife* **5**, (2016).
573 8. Sperling, M. A. *Pediatric Endocrinology-Mean Sex Steriod Concentration in Infants,*
574 *Children and adults.* (Elsevier Health Sciences, 2014).
575 9. Barbosa-Desongles, A., Hernández, C., Simó, R. & Selva, D. M. Testosterone induces
576 cell proliferation and cell cycle gene overexpression in human visceral preadipocytes. *Am. J.*
577 *Physiol., Cell Physiol.* **305**, C355-359 (2013).
578 10. Fu, R. *et al.* Novel evidence that testosterone promotes cell proliferation and
579 differentiation via G protein-coupled receptors in the rat L6 skeletal muscle myoblast cell line. *J.*
580 *Cell. Physiol.* **227**, 98–107 (2012).
581 11. Rodríguez-Lozano, D. C., Piña-Medina, A. G., Hansberg-Pastor, V., Bello-Alvarez, C. &
582 Camacho-Arroyo, I. Testosterone Promotes Glioblastoma Cell Proliferation, Migration, and
583 Invasion Through Androgen Receptor Activation. *Front. Endocrinol.* **10**, (2019).
584 12. Maasberg, M. *et al.* Androgen receptors, androgen-dependent proliferation, and 5 alpha-
585 reductase activity of small-cell lung cancer cell lines. *Int. J. Cancer* **43**, 685–691 (1989).
586 13. Allil, P. A. A., Visconti, M. A. & Isoldi, A. M. L. C. and M. C. Photoperiod and
587 Testosterone Modulate Growth and Melanogenesis of S91 Murine Melanoma. *Medicinal*
588 *Chemistry* http://www.eurekaselect.com/82341/article (2008).
589 14. Meeth, K., Wang, J. X., Micevic, G., Damsky, W. & Bosenberg, M. W. The YUMM
590 lines: a series of congenic mouse melanoma cell lines with defined genetic alterations. *Pigment*
591 *Cell Melanoma Res* **29**, 590–597 (2016).
592 15. Gao, W., Bohl, C. E. & Dalton, J. T. Chemistry and Structural Biology of Androgen
593 Receptor. *Chem Rev* **105**, 3352–3370 (2005).
594 16. Askew, E. B., Gampe, R. T., Stanley, T. B., Faggart, J. L. & Wilson, E. M. Modulation of
595 Androgen Receptor Activation Function 2 by Testosterone and Dihydrotestosterone. *J. Biol.*
596 *Chem.* **282**, 25801–25816 (2007).
597 17. Berg, A. H., Rice, C. D., Rahman, M. S., Dong, J. & Thomas, P. Identification and
598 characterization of membrane androgen receptors in the ZIP9 zinc transporter subfamily: I.
599 Discovery in female atlantic croaker and evidence ZIP9 mediates testosterone-induced apoptosis
600 of ovarian follicle cells. *Endocrinology* **155**, 4237–4249 (2014).
601 18. Matsuura, W. *et al.* SLC39A9 (ZIP9) regulates zinc homeostasis in the secretory
602 pathway: characterization of the ZIP subfamily I protein in vertebrate cells. *Biosci. Biotechnol.*
603 *Biochem.* **73**, 1142–1148 (2009).

604 19. Fatfat, M. *et al.* Copper chelation selectively kills colon cancer cells through redox
605 cycling and generation of reactive oxygen species. *BMC Cancer* **14**, 527 (2014).
606 20. He, L. *et al.* ZIP8, member of the solute-carrier-39 (SLC39) metal-transporter family:
607 characterization of transporter properties. *Mol. Pharmacol.* **70**, 171–180 (2006).
608 21. Leal, M. F. *et al.* Clinical implication of 14-3-3 epsilon expression in gastric cancer.
609 *World J. Gastroenterol.* **18**, 1531–1537 (2012).
610 22. Ruas, M. & Peters, G. The p16INK4a/CDKN2A tumor suppressor and its relatives.
611 *Biochim. Biophys. Acta* **1378**, F115-177 (1998).
612 23. Germann, U. A. *et al.* Targeting the MAPK Signaling Pathway in Cancer: Promising
613 Preclinical Activity with the Novel Selective ERK1/2 Inhibitor BVD-523 (Ulixertinib). *Mol.*
614 *Cancer Ther.* **16**, 2351–2363 (2017).
615 24. Han, Y. Analysis of the role of the Hippo pathway in cancer. *Journal of Translational*
616 *Medicine* **17**, 116 (2019).
617 25. Zhao, B., Li, L., Tumaneng, K., Wang, C.-Y. & Guan, K.-L. A coordinated
618 phosphorylation by Lats and CK1 regulates YAP stability through SCFβ-TRCP. *Genes Dev* **24**,
619 72–85 (2010).
620 26. Fujii, M. Exploration of a new drug that targets YAP. *J. Biochem.* **152**, 209–211 (2012).
621 27. Bulldan, A., Malviya, V. N., Upmanyu, N., Konrad, L. & Scheiner-Bobis, G.
622 Testosterone/bicalutamide antagonism at the predicted extracellular androgen binding site of
623 ZIP9. *Biochim Biophys Acta Mol Cell Res* **1864**, 2402–2414 (2017).
624 28. Ponnusamy, S. *et al.* Orally-Bioavailable Androgen Receptor Degrader, A Potential
625 Next-Generation Therapeutic for Enzalutamide-Resistant Prostate Cancer. *Clin. Cancer Res.*
626 (2019) doi:10.1158/1078-0432.CCR-19-1458.
627 29. Chi, K. N. *et al.* Apalutamide for Metastatic, Castration-Sensitive Prostate Cancer. *N.*
628 *Engl. J. Med.* **381**, 13–24 (2019).
629 30. Kayigil, O., Atahan, O. & Metin, A. Cyproterone acetate monotherapy in advanced
630 prostatic carcinoma. *Int Urol Nephrol* **29**, 213–220 (1997).
631 31. Fukada, T. & Kambe, T. Molecular and genetic features of zinc transporters in
632 physiology and pathogenesis. *Metallomics* **3**, 662–674 (2011).
633 32. Costello, L. C., Liu, Y., Zou, J. & Franklin, R. B. Evidence for a zinc uptake transporter
634 in human prostate cancer cells which is regulated by prolactin and testosterone. *J Biol Chem* **274**,
635 17499–17504 (1999).
636 33. Bafaro, E., Liu, Y., Xu, Y. & Dempski, R. E. The emerging role of zinc transporters in
637 cellular homeostasis and cancer. *Signal Transduction and Targeted Therapy* **2**, 1–12 (2017).
638 34. Ma, M. *et al.* Sustained androgen receptor signaling is a determinant of melanoma cell
639 growth potential and tumorigenesis. *J Exp Med* **218**, (2021).
640 35. Klein, S. L. & Flanagan, K. L. Sex differences in immune responses. *Nat. Rev. Immunol.*
641 **16**, 626–638 (2016).
642

643

644

645

646 **Figure legends**

647 **Fig. 1: Biologic sex and testosterone promote proliferation of melanoma models lacking**
648 **detectable AR.** Tumor growth of human WM46 melanoma in male and female immunodeficient
649 SCID mice. Tumor doubling times are 16.2 and 18.6 days for males and females respectively
650 (Non-linear regression analysis/Exponential fit. See also Sup. Fig. 1 for expanded statistical
651 analysis). **B.** Cell proliferation (cell number) determined after 6 days of treatment with vehicle
652 (DMSO), 100nM testosterone (T) or 100nM dihydrotestosterone (DHT). Human primary
653 melanocytes (H.Mel.) and human melanoma WM46 cells are shown. Graphs represent the
654 average of three independent experiments. **C.** Cell proliferation of human WM46 and murine
655 YUMM1.7 melanoma cells exposed to increasing concentrations of testosterone (T) (left panels)
656 or dihydrotestosterone (DHT) (right panel). **D.** AR mRNA expression in primary melanocytes
657 (L: low melanin content; D: High melanin content), a battery of human melanoma lines, and
658 murine YUMM1.7 determined by qPCR. VCaP cell line (prostate cancer) was used as a positive
659 control. **E.** AR protein expression determined by Western blot with two different antibodies.
660 Upper line = Androgen Receptor [(D6F11) XP® Rabbit mAb #5153. Lower line = Recombinant
661 Anti-Androgen Receptor antibody [EPR1535(2)] (ab133273). Two human prostate cancer lines
662 were used as a positive control (VCaP and LNCaP). β-actin was used as loading control.
663 ** p value≤0.01; * p value≤0.05.
664

665 **Fig 2: ZIP9 is active in human melanoma cells, and is broadly expressed in human**
666 **melanocytic tumors. A.** ZIP9 protein expression determined by western blot in primary
667 melanocytes and a battery of human melanoma cell lines. **B.** Time-lapse *in vivo* analysis of Zn^{++}
668 influx in WM46 cells upon testosterone addition (100nM). FluoZin-3 was used as Zn^{++} reporter.
669 **C.** Intracellular levels of Zn^{++} after long-term testosterone treatment (96 hours; 100nM

670 testosterone). Zinc levels were measured as fluorescence intensity per cell. FluoZin-3 was used
671 as Zn^{++} reporter. Representative images are shown on the right at indicated time-points. **D.**
672 WM46 relative proliferation (cell number) after 6 days in the presence of 100 nM testosterone
673 (T) +/- 200 nM zinc chelator (TPEN). **E.** WM46 proliferation in the presence exogenous divalent
674 cations Zn^{++} Fe^{++} and Mn^{++}. Cells were grown for 6 days and treated as indicated in the legend.
675 Error bars represent standard error of the mean (SEM). **F.** Validation of ZIP9 [(SLC39A9
676 Antibody (PA5-52485)] and androgen receptor [(Leica AR-318-L-CE, clone AR27 (clone AR27,
677 1:25)] antibodies for immunohistochemistry. ZIP9 staining performed in wild-type and ZIP9
678 knock-out cells. Prostate gland tissue and human prostate cancer samples were used as positive
679 controls for AR. Representative images of human melanoma samples stained for ZIP9 and AR.
680 Tumors expressing low, medium and high levels of ZIP9 are shown. Replicates from the same
681 samples stained for AR are shown. 20X magnification (1.6X zoom). Scale bar=60μM. **G.**
682 Graphic representation of the % of tumors that express ZIP9. Data from nevus, primary
683 melanomas and metastatic melanoma are displayed. **H.** Graphic representation of the percentage
684 of nevi, primary lesions and metastatic tumors classified according to ZIP9 intensity (Score 1=1-
685 25%, 2=26-50%, 3=51-75%, 4=76-100%).
686 **** p value≤0.0001; ** p value≤0.01; * p value≤0.05; n.s>0.05.
687
688 **Fig. 3: ZIP9 mediates testosterone effects in melanoma. A.** Proliferation (cell number) of
689 isogenic clonal populations of WM46 wtZIP9 and ΔZIP9 (gRNA #3) cells exposed to increasing
690 concentrations of testosterone (T) and dihydrotestosterone (DHT). **B.** Proliferation (cell number)
691 of isogenic clonal populations of WM46 wtZIP9 and ΔZIP9 (gRNA #4) cells exposed to
692 increasing concentrations of testosterone (T) and dihydrotestosterone (DHT). The graph
693 represents the average of three independent experiments. **C.** Intracellular levels of zinc in human

694 melanoma ΔZIP9 cells measured as relative fluorescence intensity of FluoZin-3. Graphs
695 represent the average of three independent experiments. **D.** Relative cell proliferation in the
696 presence of 100nM testosterone (T), zinc chelator (200nM TPEN) and $ZnCl_2$ (400nM). Cells
697 were cultured for 6 days. The graph represents the average of three independent experiments.
698 **** p value≤0.0001; ** p value≤0.01; * p value≤0.05; n.s>0.05.
699
700 **Fig. 4: Testosterone driven increase in melanoma proliferation requires ZIP9 and**
701 **activation of MAPK and YAP1. A.** RPPA analysis displaying changes in protein expression in
702 WM46 human melanoma cells following exposure to 100 nM testosterone (T) for increasing
703 amounts of time. Down-regulated proteins are shown in green; red color corresponds to up-
704 regulated proteins and control proteins showing no fold-change when compared to vehicle-
705 treated cells are shown in blue. **B.** Relative proliferation (cell number) after exposure to
706 pharmacologic ERK1/2 inhibition via 50nM RVD-523 (Ei) alone or in combination with
707 testosterone. wtZIP9 and ΔZIP9 WM46 cells are shown. The western blot shows levels of
708 phosphorylation of the ERK target RSK in wtZIP9 and ΔZIP9 WM46 cells (Ei represents RVD-
709 523). **C.** Western blot for YAP1 in fractionated WM46 lysates. Cells were treated with 100 nM
710 testosterone for the indicated times. β-Actin is used as cytoplasmic fraction positive control.
711 PARP is used as nuclear fraction positive control. **D.** Quantification of YAP-1 nuclear
712 immunodetection after 30 minutes of exposure to 100 nM testosterone (T) and/or 8μM
713 dobutamine (Dob) in wtZIP9 and ΔZIP9 cells. **E.** Proliferation of wtZIP9 and ΔZIP9 WM46
714 cells after treatment with 100nM testosterone (T) and/or the YAP inhibitor dobutamine (Dob). **F.**
715 Relative mRNA expression of YAP1 target genes after 30 minutes in the presence of 100 nM
716 testosterone and/or 8μM dobutamine. Error bars represent standard error of the mean (SEM).

717 *** p value≤0.001; ** p value≤0.01; * p value≤0.05; n.s>0.05.

718

719 **Fig. 5: Pharmacologic ZIP9 blockade inhibits melanoma *in vivo*. A.** Proliferation of human
720 melanoma cells (WM46) in the presence of 100 nM testosterone (T) +/- 2 μM AR inhibitors
721 (BIC:Bicalutamide; ENZ:Enzalutamide; APA:Apalutamide). Western blot showing ERK and p-
722 ERK proteins in WM46 cells treated with 100nM testosterone +/- 2μM BIC +/- 200 nM zinc
723 chelator (TPEN). **B.** Cell proliferation in human and murine derived melanoma cells (SK-MEL-
724 3, SK-MEL-2 and YUMM1.7) treated with 100 nM testosterone (T) in combination with
725 apalutamide (2 μM) (APA). **C.** Cell membrane labeling with cell impermeable testosterone-BSA
726 conjugated with FITC (0.25 μM). BSA-FITC (0.25 μM) was used as a negative control for
727 unspecific binding. Quantification of membrane labeling with T-BSA or the control BSA. The
728 graph represents the fluorescence intensity relative to the total area of each cell. **D.** Proliferation
729 of WM46 wtZIP9 and ΔZIP9 treated with 100 nM testosterone (T) in combination with
730 apalutamide (2 μM) (APA). **E.** Tumor growth and survival analysis in SCID male mice bearing
731 WM46 derived subcutaneous tumors (APA treatment: 20 mg/kg/day via oral gavage). ** p-
732 value<0.005 by ANOVA. Doubling time (non-linear regression analysis): Vehicle=11.11 days;
733 APA=25.22 days. **F.** Working model: ZIP9 activation promotes ERK phosphorylation and
734 induces YAP1 nuclear translocation. AR inhibitors [represented in the figure by apalutamide
735 (APA)] block testosterone effects through ZIP9 inactivation.
736 **** p value≤0.0001; *** p value≤0.001; ** p value≤0.01; * p value≤0.05; n.s>0.05.

737

738

739

740 **Figures**

Figure 1

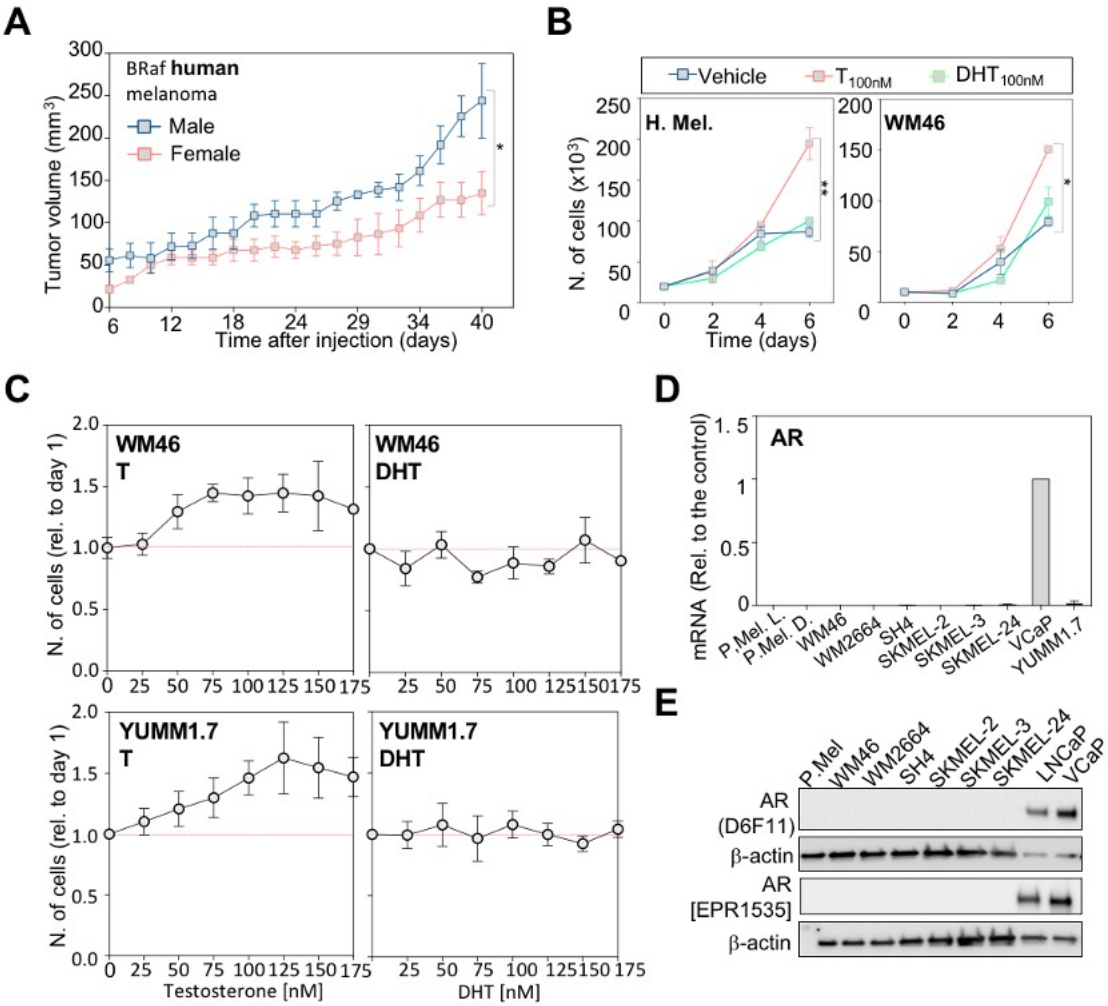

741

Figure 2

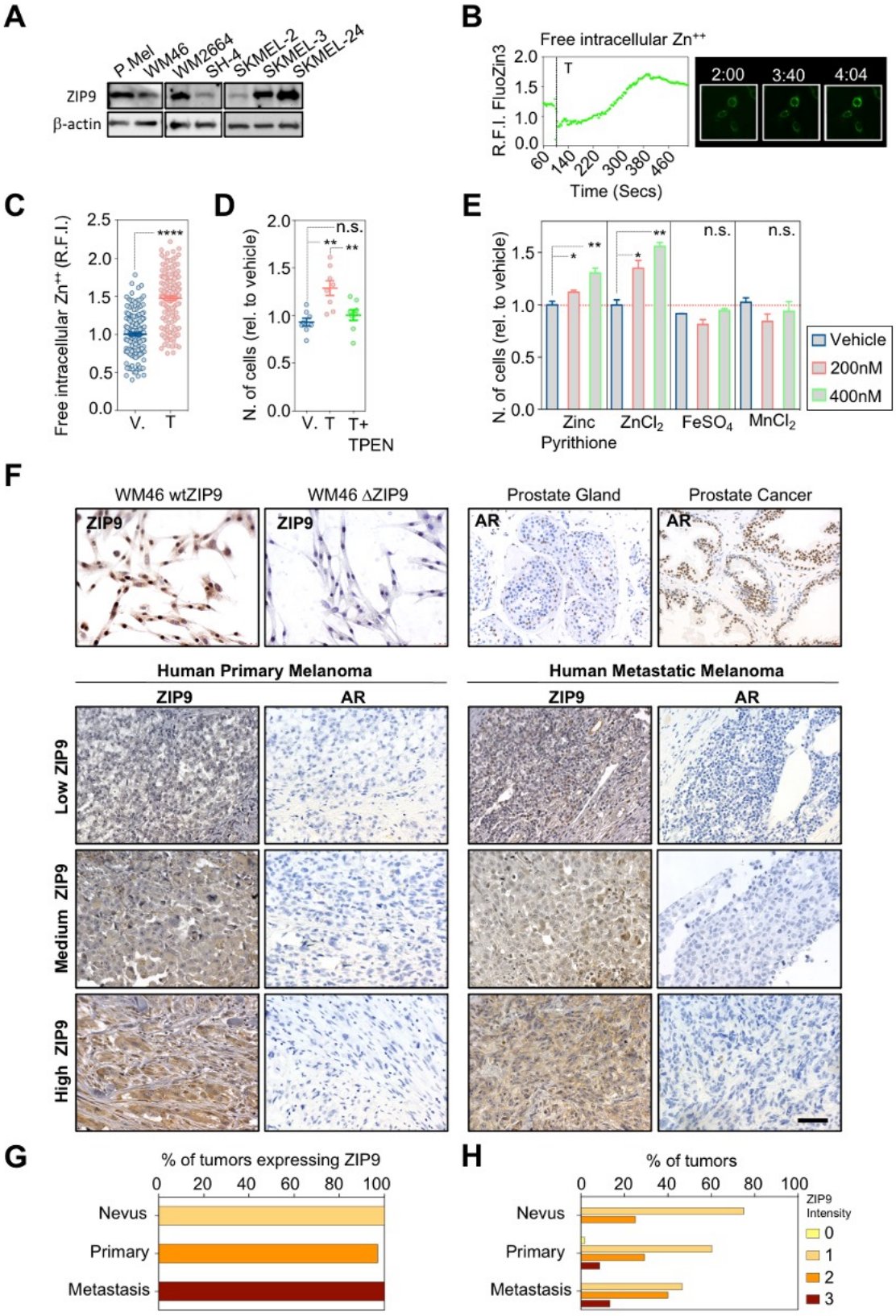
A
P.Mel
WM46
WM2664
SH-4
SKMEL-2
SKMEL-3
SKMEL-24
ZIP9
β-actin
B
Free intracellular Zn++
R.F.I. FluoZin3
T
2:00
3:40
4:04
Time (Secs)
C
Free intracellular Zn++ (R.F.I.)
****
V.
T
D
N. of cells (rel. to vehicle)
n.s.
**
**
V.
T
T+ TPEN
E
N. of cells (rel. to vehicle)
Zinc Pyrithione
ZnCl2
FeSO4
MnCl2
Vehicle
200nM
400nM
F
WM46 wtZIP9
WM46 ΔZIP9
Prostate Gland
Prostate Cancer
ZIP9
AR
Human Primary Melanoma
Human Metastatic Melanoma
Low ZIP9
Medium ZIP9
High ZIP9
G
% of tumors expressing ZIP9
Nevus
Primary
Metastasis
H
% of tumors
ZIP9 Intensity
0
1
2
3

742

Figure 3

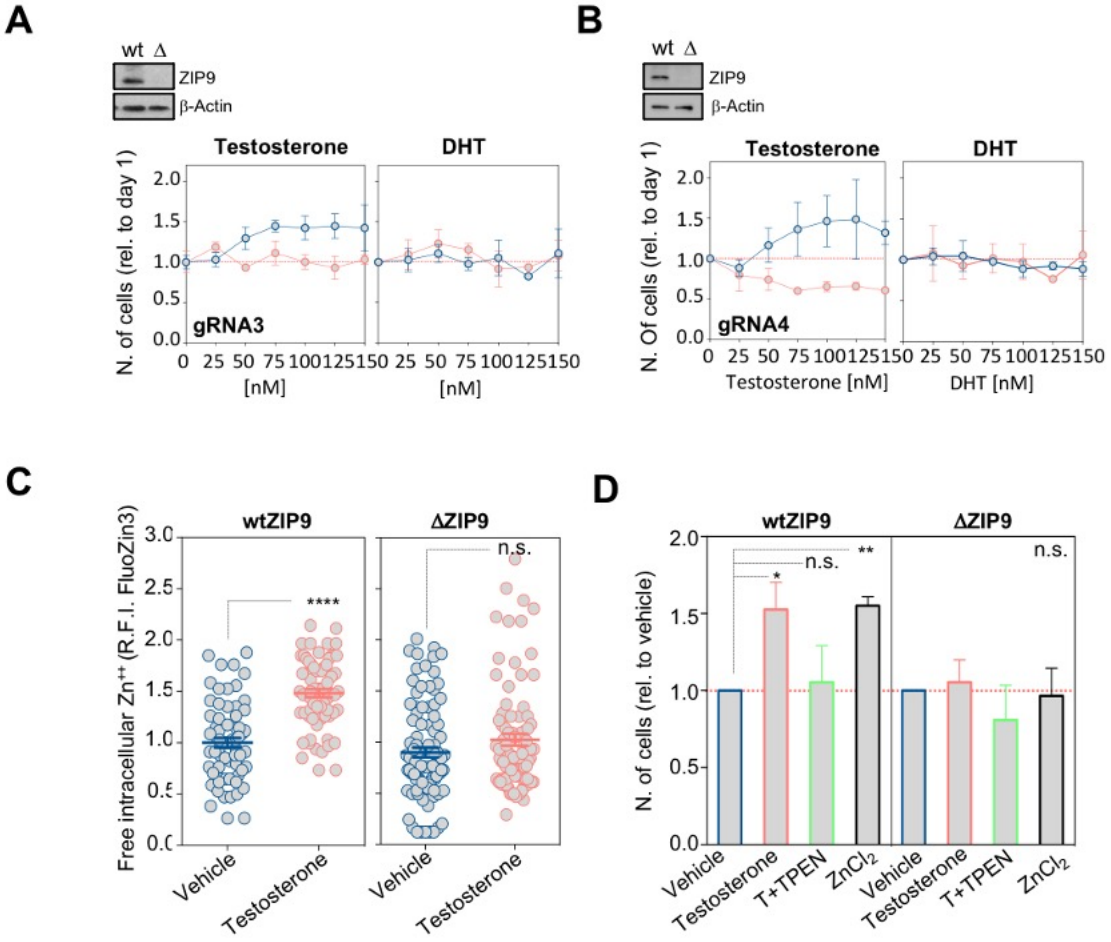

743

744
745
746
747

Figure 4

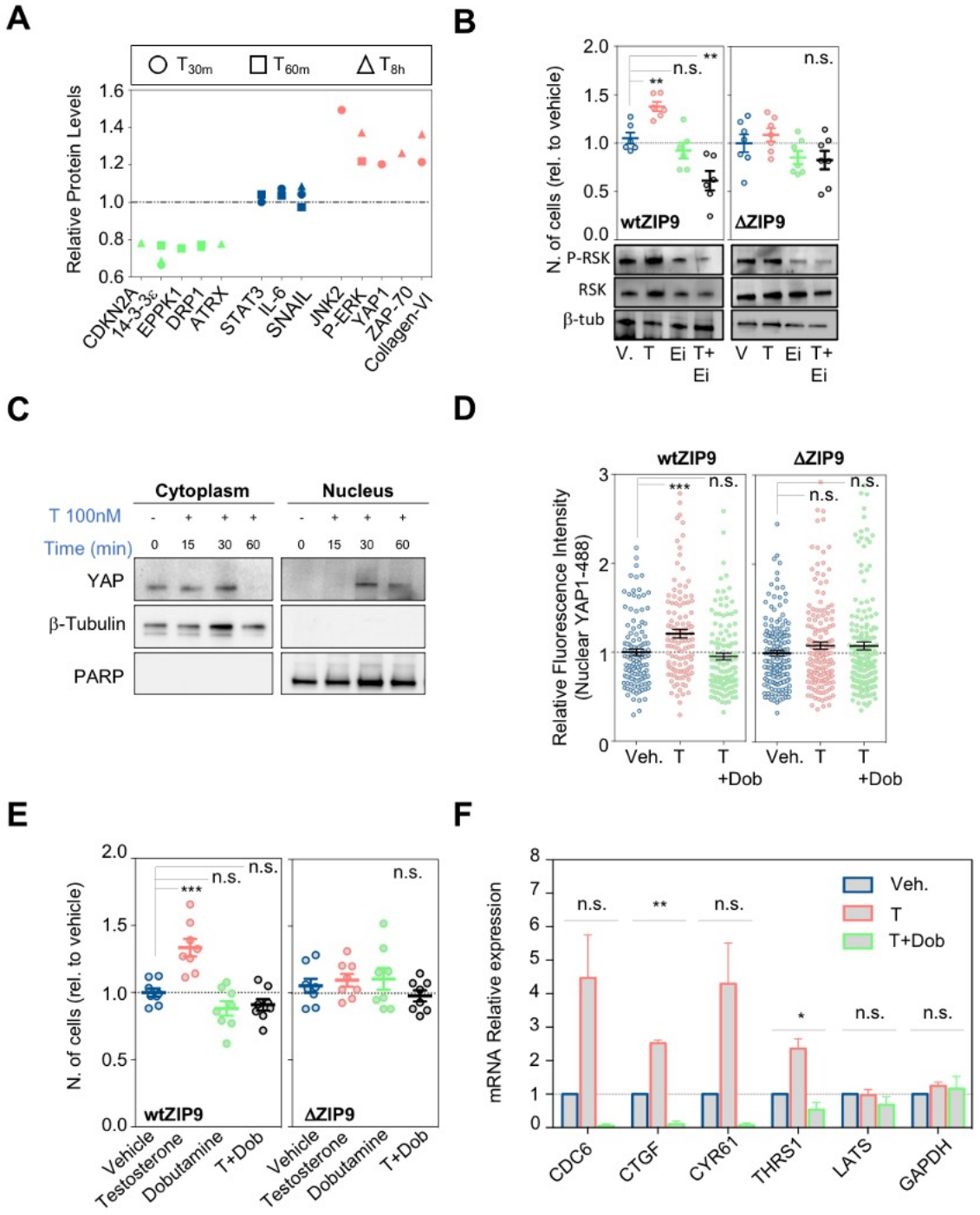
A
T30m
T60m
T8h
Relative Protein Levels
CDKN2A
14-3-3ε
EPPK1
DRP1
ATRX
STAT3
IL-6
SNAIL
JNK2
P-ERK
YAP1
ZAP-70
Collagen-VI
B
N. of cells (rel. to vehicle)
n.s.
**
wtZIP9
ΔZIP9
P-RSK
RSK
β-tub
V. T Ei T+ Ei
V T Ei T+ Ei
C
Cytoplasm
Nucleus
T 100nM
Time (min)
0 15 30 60
YAP
β-Tubulin
PARP
D
wtZIP9
ΔZIP9
Relative Fluorescence Intensity (Nuclear YAP1-488)
***
n.s.
Veh. T T +Dob
E
N. of cells (rel. to vehicle)
***
n.s.
wtZIP9
ΔZIP9
Vehicle
Testosterone
Dobutamine
T+Dob
F
mRNA Relative expression
Veh.
T
T+Dob
n.s.
**
*
CDC6
CTGF
CYR61
THRS1
LATS
GAPDH

748

Figure 5

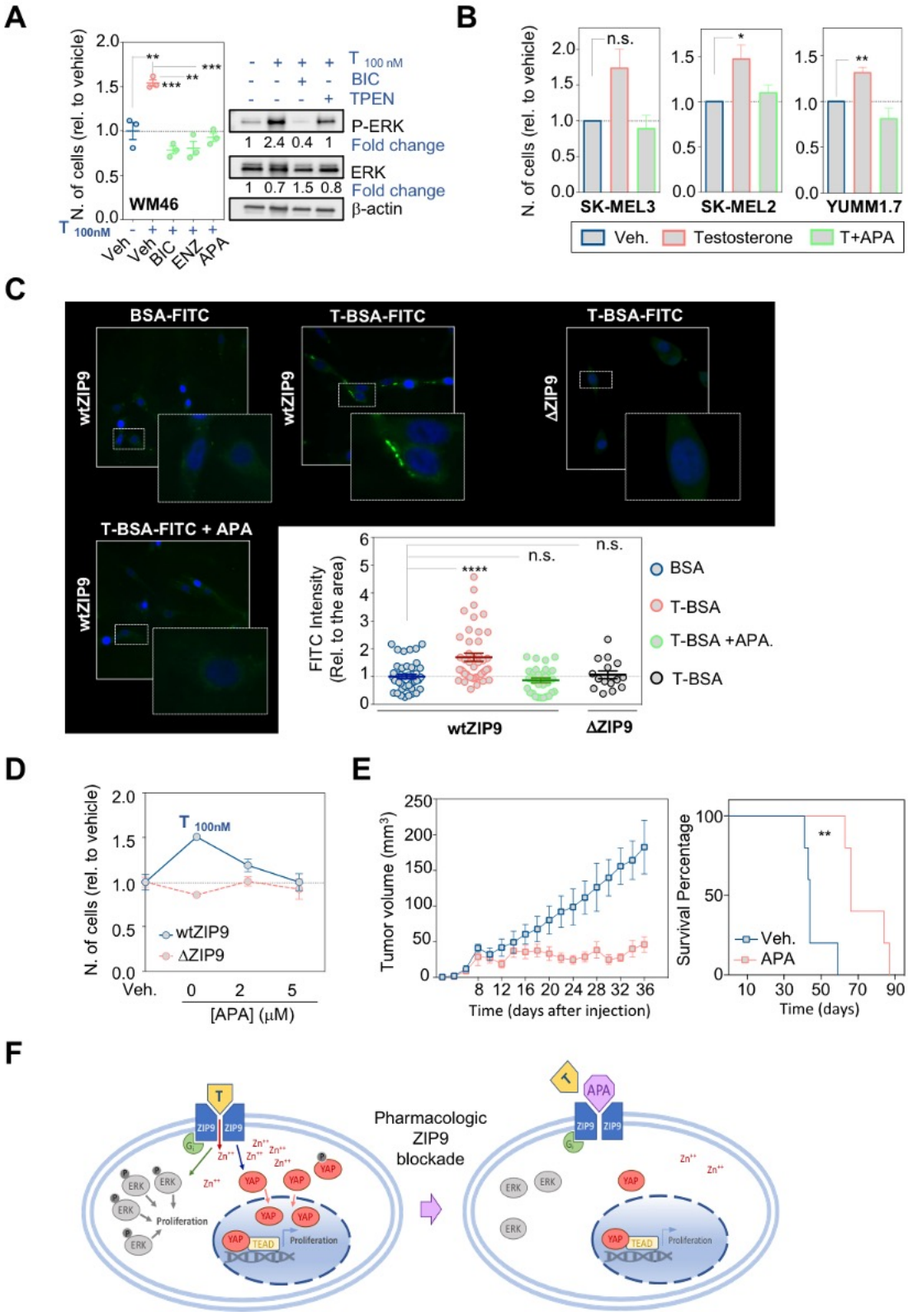
A
N. of cells (rel. to vehicle)
WM46
T 100nM
Veh
Veh
BIC
ENZ
APA
T 100 nM
BIC
TPEN
P-ERK
Fold change
1 2.4 0.4 1
ERK
Fold change
1 0.7 1.5 0.8
β-actin
B
N. of cells (rel. to vehicle)
n.s.
SK-MEL3
SK-MEL2
YUMM1.7
Veh.
Testosterone
T+APA
C
BSA-FITC
T-BSA-FITC
T-BSA-FITC
T-BSA-FITC + APA
wtZIP9
ΔZIP9
FITC Intensity (Rel. to the area)
n.s.
BSA
T-BSA
T-BSA +APA.
T-BSA
wtZIP9
ΔZIP9
D
N. of cells (rel. to vehicle)
T 100nM
wtZIP9
ΔZIP9
Veh.
[APA] (μM)
E
Tumor volume (mm³)
Time (days after injection)
Survival Percentage
Veh.
APA
Time (days)
F
T
ZIP9
ERK
YAP
TEAD
Proliferation
Pharmacologic ZIP9 blockade
APA

749

750 **Supplementary Figures**

Supplementary Figure 1

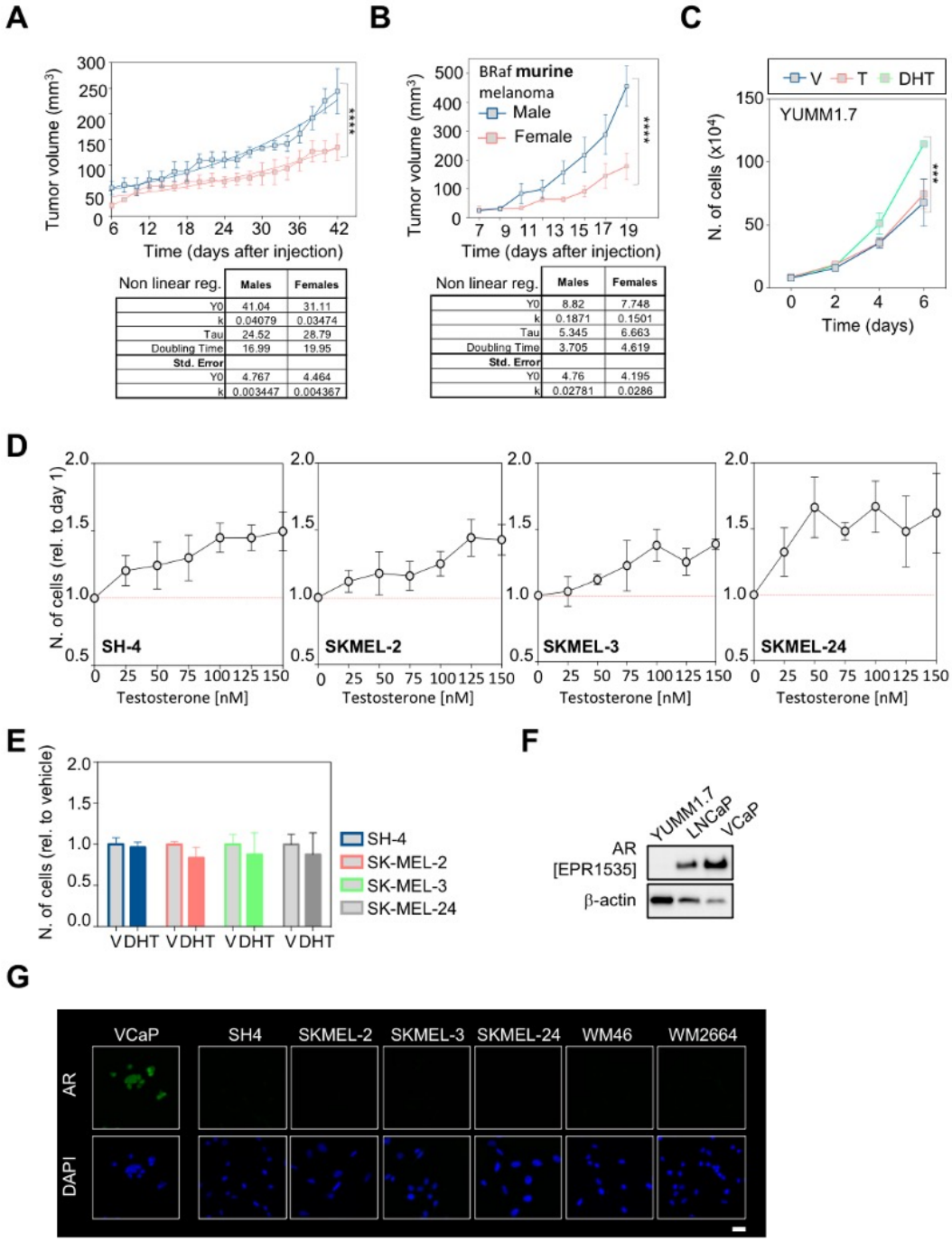

Non linear reg.	Males	Females
Y0	41.04	31.11
k	0.04079	0.03474
Tau	24.52	28.79
Doubling Time	16.99	19.95
Std. Error		
Y0	4.767	4.464
k	0.003447	0.004367

Non linear reg.	Males	Females
Y0	8.82	7.748
k	0.1871	0.1501
Tau	5.345	6.663
Doubling Time	3.705	4.619
Std. Error		
Y0	4.76	4.195
k	0.02781	0.0286

751
752

753 **Fig. S1.** Non-linear regression analysis (Exponential fit) for males and females. Doubling time
754 for tumor growth: males=16.99 days and females=19.95 days. (Linear-regression analysis for
755 slope comparison: **** p-value<0.0001). **B.** Tumor growth in C57BL/6 male and female mice
756 bearing syngeneic murine melanoma (YUMM1.7). Doubling time for tumor growth: males = 3.7
757 days, females = 4.6 days (Linear-regression analysis for slope comparison: **** p-
758 value<0.0001). **C.** YUMM1.7 cell number determined after 6 days of treatment with vehicle
759 (DMSO), 100 nM testosterone (T) or 100 nM dihydrotestosterone (DHT). Graphs represent the
760 average of three independent experiments. Error bars represent standard error of the mean
761 (SEM). **D.** Relative cell proliferation of human melanoma cell lines treated for 6 days with
762 increasing concentrations of testosterone (T). **E.** Relative cell proliferation of human melanoma
763 cells treated for 6 days with dihydrotestosterone (DHT 100 nM). **F.** AR protein expression
764 determined by Western blot in YUMM1.7 cells. **G.** Immunofluorescence detecting AR (D6F11)
765 in a battery of human-derived melanoma cells. AR is shown in green; DNA was stained with
766 DAPI and it is shown in blue. Scale bar 25μM. Error bars represent standard error of the mean
767 (SEM). **** p value≤0.0001; *** p value≤0.001.
768 .
769
770
771
772
773
774
775

Supplementary Figure 2

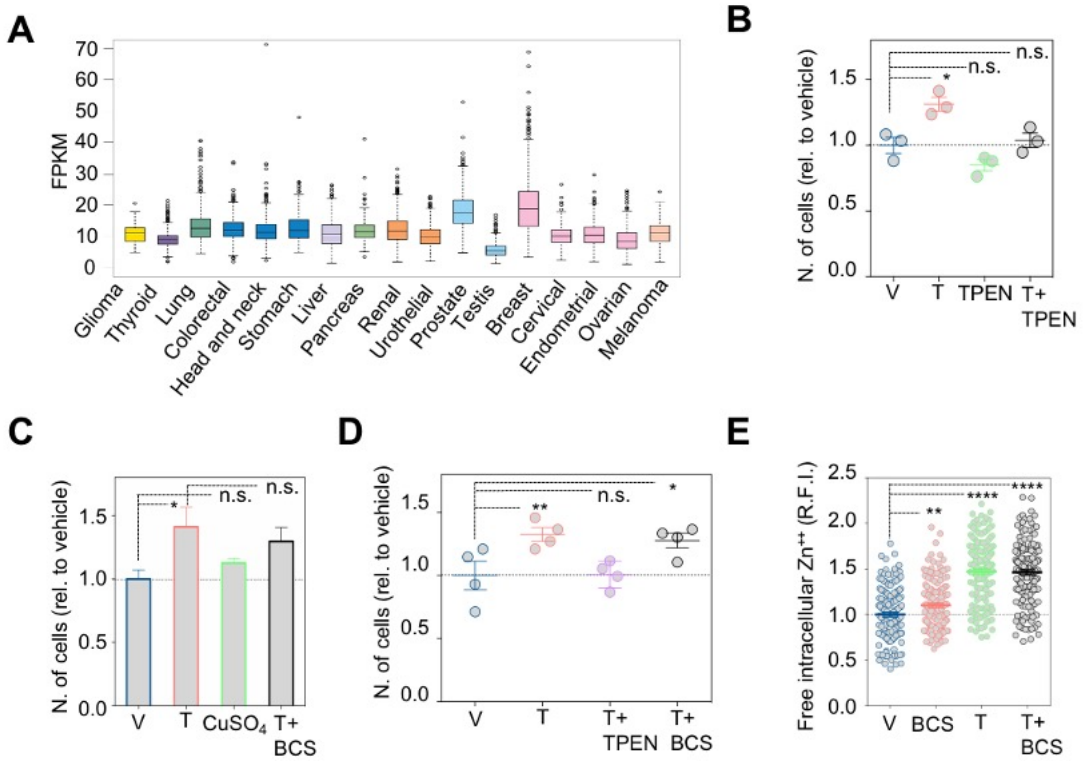

Fig. S2. A. RNA-seq data from 17 cancer types reported as median FPKM (number Fragments Per Kilobase of exon per Million reads), generated by the The Cancer Genome Atlas (TCGA). RNA cancer tissue category calculated based on mRNA expression levels across all 17 cancer tissues and include: cancer tissue enriched, cancer group enriched, cancer tissue enhanced, expressed in all, mixed and not detected. Normal distribution across the dataset is visualized with box plots, shown as median and 25th and 75th percentiles. Points are displayed as if they are above or below 1.5 times the interquartile range. **B.** WM46 relative proliferation (cell number) in presence of 100 nM testosterone (T) +/- 200 nM zinc chelator TPEN. **C.** WM46 proliferation treated with 100 nM testosterone (T), +/- copper sulfate (CuSO4) and copper chelator (25µM BCS). **D.** Relative cell proliferation of WM46 cells treated with testosterone (100nM) +/- zinc chelator TPEN (200nM) and the copper chelator BCS (25µM). **E.** Relative intracellular Zn^{++} in

788 cells treated with testosterone and/or copper chelator (BCS). The graph represents relative
789 fluorescence intensity. Error bars represent standard error of the mean (SEM).
790 **** p value≤0.0001; ** p value≤0.01; * p value≤0.05; n.s>0.05.
791
792
793
794
795
796
797
798
799
800
801
802
803
804
805
806
807
808
809
810

Supplementary Figure 3

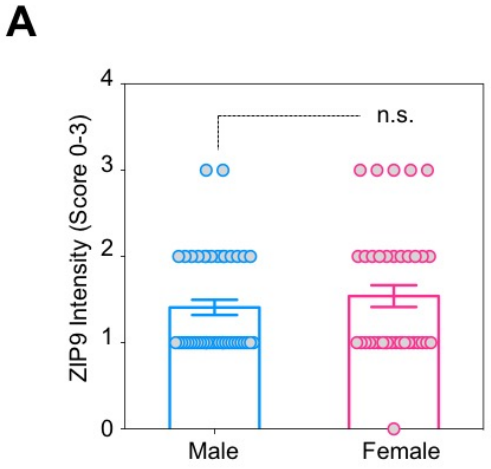

Fig. S3. Graphic representation of ZIP9 staining intensity in human samples from nevus, primary melanoma and metastatic melanoma in males vs. females (Score 1=1-25%, 2=26-50%, 3=51-75%, 4=76-100%). n.s>0.05.

Supplementary Figure 4

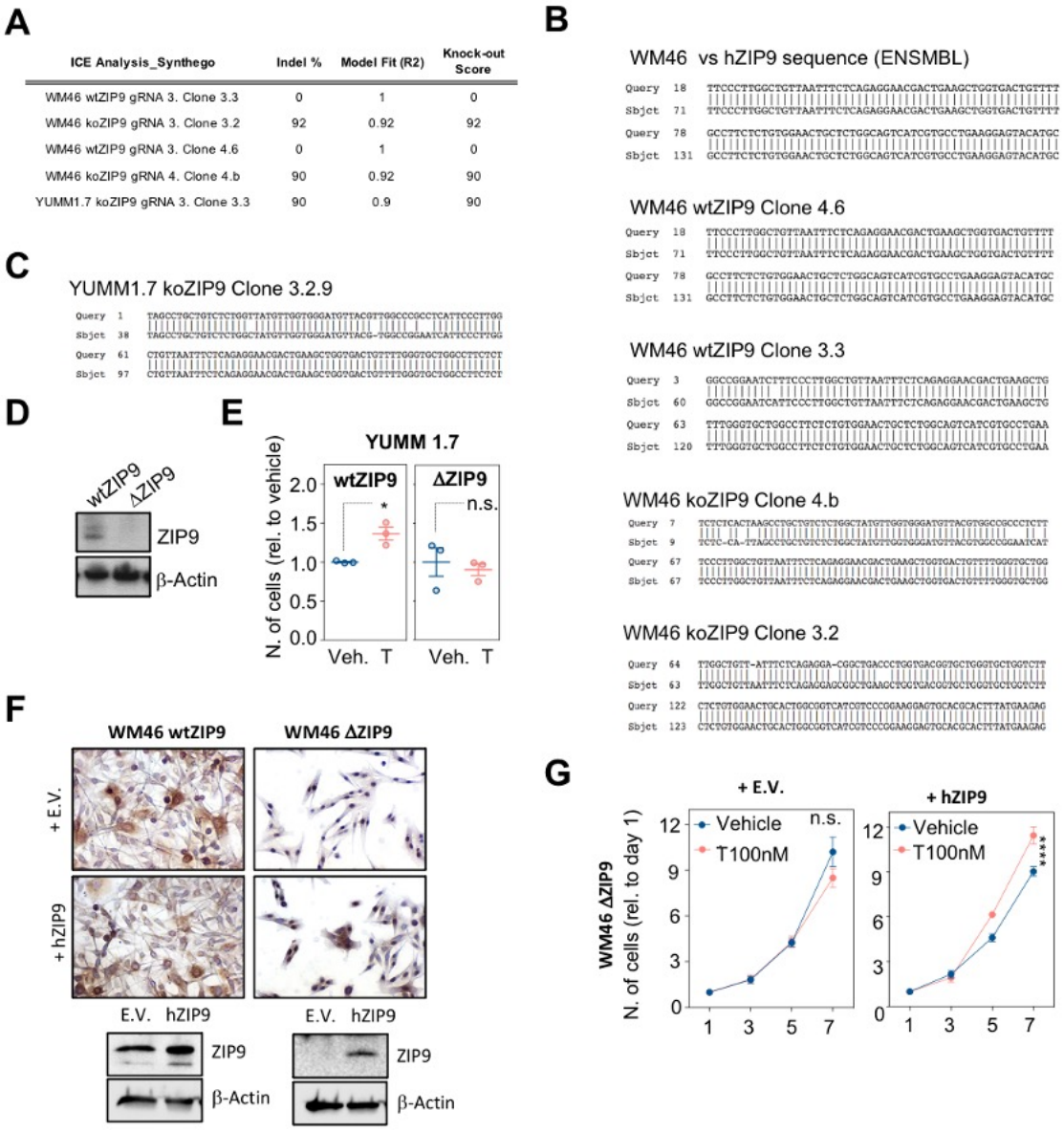

ICE Analysis_Synthego	Indel %	Model Fit (R2)	Knock-out Score
WM46 wtZIP9 gRNA 3. Clone 3.3	0	1	0
WM46 koZIP9 gRNA 3. Clone 3.2	92	0.92	92
WM46 wtZIP9 gRNA 3. Clone 4.6	0	1	0
WM46 koZIP9 gRNA 4. Clone 4.b	90	0.92	90
YUMM1.7 koZIP9 gRNA 3. Clone 3.3	90	0.9	90

Fig. S4. A. Table shows the knock-out scores for WM46 isogenic clones obtained using ICE Analysis software (Synthego). **B.** Blast alignment of the DNA sequences surrounding the gRNA target sequence and SLC39A9 (Ensmbl. Homo Sapiens_SLC39A9_202) are shown for each isogenic clone. As control for the sequencing, WM46 parental cells were sequenced and aligned

841 with human SLC39A9 (Ensmbl. Homo Sapiens_SLC39A9_202). Query = SLC39A9_202; Sbjct
842 = isogenic clone sequences **C.** Target sequence of YUMM1.7 isogenic clone was aligned with
843 *mus musculus* Slc30a9 sequence**. D.** Western blot showing ZIP9 expression in wild type and
844 knock-out YUMM1.7 isogenic clones. **E.** Relative proliferation (cell number) of YUMM1.7
845 wtZIP9 and ΔZIP9 in the presence of 100 nM testosterone (T) for 6 days. The graphs represent
846 the average of three independent experiments. Error bars represent standard error of the mean
847 (SEM). * p value≤0.05. **F.** Immunocytochemistry in WM46 isogenic clones transduced with
848 control pRRL lentivector (E.V.) or hZIP9 expressing lentivector. Western blots below show the
849 proteins in each sample 72 hours after transduction. **G.** Relative cell proliferation (cell number)
850 with testosterone treatment (100 nM) for 7 days in WM46 ΔZIP9 isogenic clones transduced
851 with empty pRRL lentivector (E.V.) (left panel) or pRRL_hZIP9 expressing vector (right panel).
852 Error bars represent standard error of the mean (SEM). **** p value≤0.0001; n.s>0.05.
853
854
855

Supplementary Figure 5

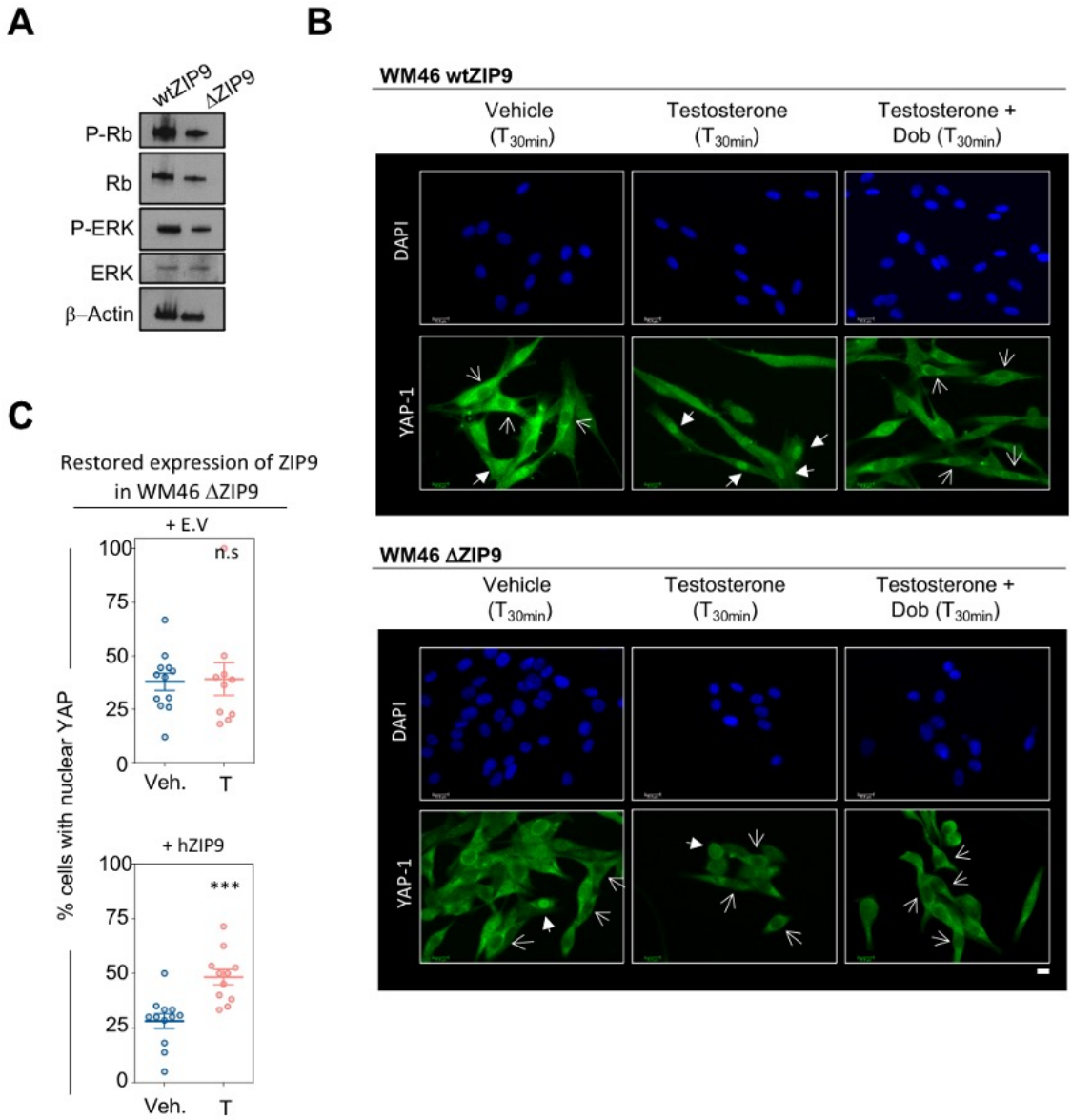

Fig. S5. A. Western blot showing baseline levels of ERK phosphorylation in wtZIP9 and ΔZIP9 WM46 cells. **B.** Representative images of YAP-1 immunodetection after 30 minutes of exposure to 100 nM testosterone (T) +/- 8μM dobutamine (Dob) in wtZIP9 and ΔZIP9 cells. The percentage of cells with nuclear YAP-1 (per field) are shown in the upper-left side of each panel. YAP1 is shown in green; β-actin is shown in red; DAPI highlights nuclear DNA in blue. Thin

863 arrows indicate cells where YAP1 is not localized inside the nucleus. Opaque arrows indicate
864 cells with nuclear YAP-1. Scale bar=15μm. **C.** Percentage of WM46 wtZIP9 and ΔZIP9 cells
865 transduced with pRRL empty vector (E.V.) or pRRL_hZIP9 expressing vector with nuclear
866 localization of YAP1. Cells were treated with vehicle and 100 nM testosterone.
867 *** p value≤0.001; n.s>0.05.
868
869
870
871

Supplementary Figure 6

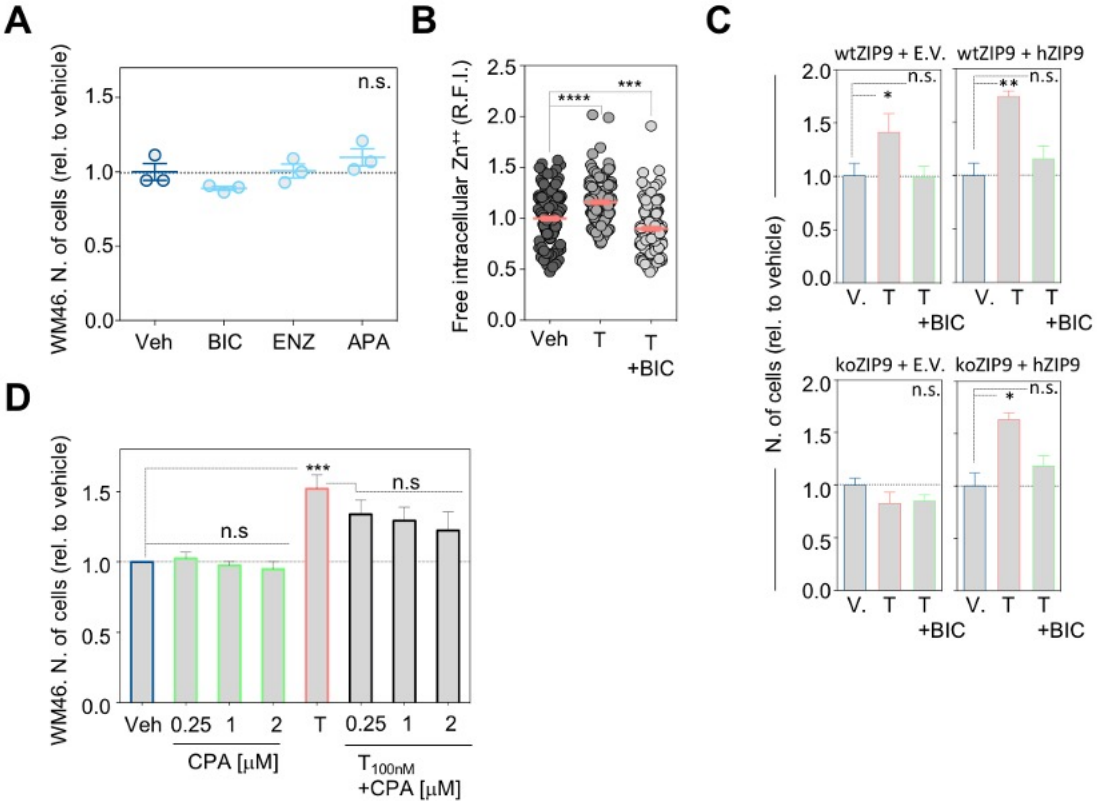

872

873 **Fig. S6. A.** Relative cell proliferation (cell number) in human-derived melanoma cells (WM46)

874 treated with 2μM AR inhibitors (BIC:Bicalutamide; ENZ:Enzalutamide; APA:Apalutamide). **B.**

875 Intracellular Zn^{++} in WM46 cells treated with 100 nM testosterone and/or 2 μM bicalutamide

876 (BIC). **C.** Relative cell proliferation (cell number) of WM46 wtZIP9 and ΔZIP9 transduced with

877 pRRL empty vector (E.V.) or pRRL_hZIP9 expressing vector. Cells were treated with vehicle

878 (V) or 100 nM testosterone +/- bicalutamide (2μM) **D**. Relative cell proliferation of WM46 cells

879 treated with 100nM testosterone and/or cyproterone acetate (CPA) for 6 days.

880 **** p value≤0.0001; *** p value≤0.001; ** p value≤0.01; * p value≤0.05; n.s>0.05.

881

Supplementary Figure 7

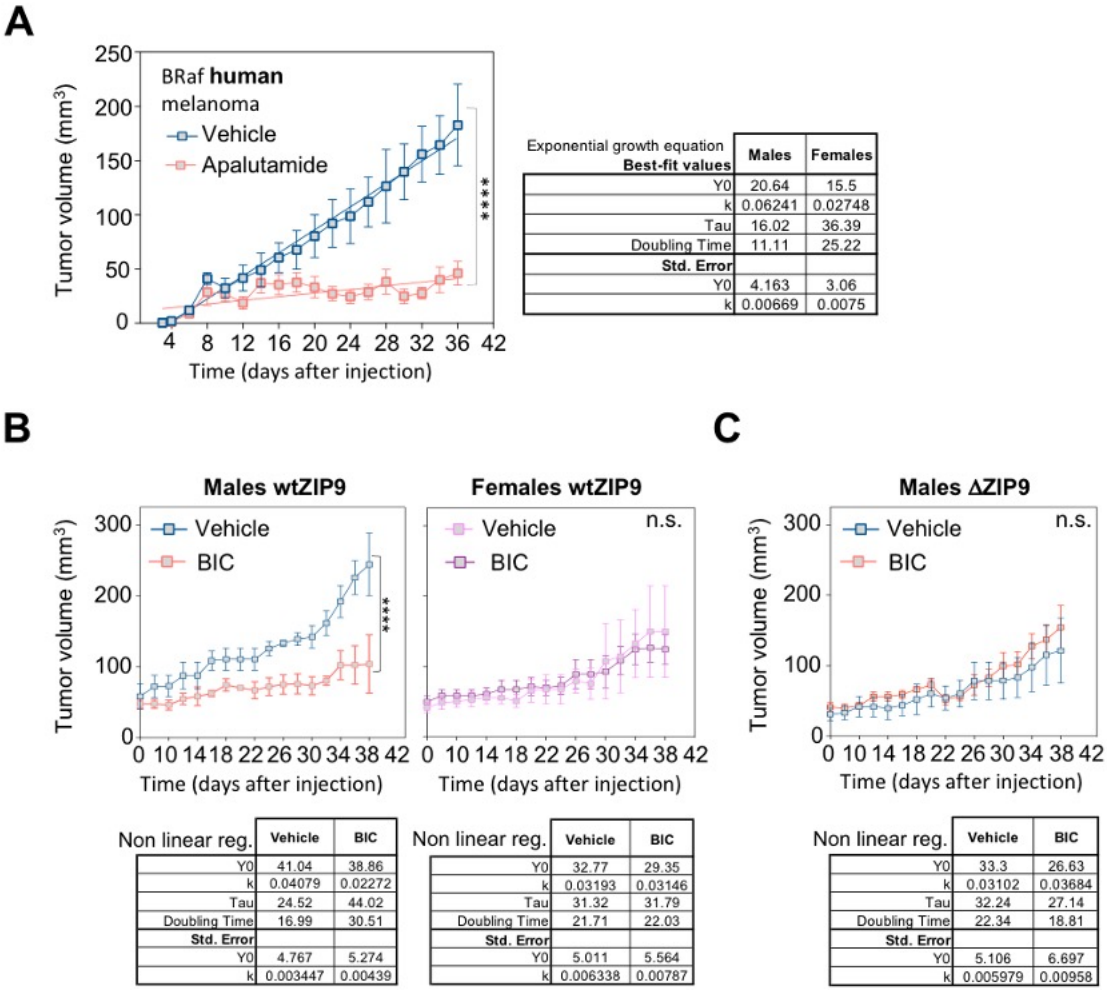

Exponential growth equation Best-fit values	Males	Females
Y0	20.64	15.5
k	0.06241	0.02748
Tau	16.02	36.39
Doubling Time	11.11	25.22
Std. Error		
Y0	4.163	3.06
k	0.00669	0.0075

Non linear reg.	Vehicle	BIC
Y0	41.04	38.86
k	0.04079	0.02272
Tau	24.52	44.02
Doubling Time	16.99	30.51
Std. Error		
Y0	4.767	5.274
k	0.003447	0.00439

Non linear reg.	Vehicle	BIC
Y0	32.77	29.35
k	0.03193	0.03146
Tau	31.32	31.79
Doubling Time	21.71	22.03
Std. Error		
Y0	5.011	5.564
k	0.006338	0.00787

Non linear reg.	Vehicle	BIC
Y0	33.3	26.63
k	0.03102	0.03684
Tau	32.24	27.14
Doubling Time	22.34	18.81
Std. Error		
Y0	5.106	6.697
k	0.005979	0.00958

Fig. S7. A. Non-lineal regression analysis (Exponential fit) for males treated with vehicle vs. APA. Doubling time for tumor growth: Vehicle treated males=16.0 days and APA treated males=36.4 days. Linear regression analysis for slope comparison demonstrate significant differences between vehicle treated and apalutamide treated males (p-value<0.0001). **B.** Tumor growth in mice bearing WM46 derived subcutaneous tumors. Daily treatment with bicalutamide (30 mg/kg/day, via oral gavage) or vehicle are shown for both male and female mice. Linear regression analysis of slopes demonstrates significant differences between vehicle treated and

890 Bic treated males (p-value<0.0001). **C.** Tumor growth in SCID male mice bearing ΔZIP9 WM46

891 melanoma. Mice were treated daily with bicalutamide (30 mg/kg/day) or vehicle via oral gavage.

892 Exponential fit analyses are included bellow each tumor growth graphical representation.

893 **** p value≤0.0001; n.s>0.05.

894
895
896
897
898
899
900
901
902
903

Supplementary Figure 8

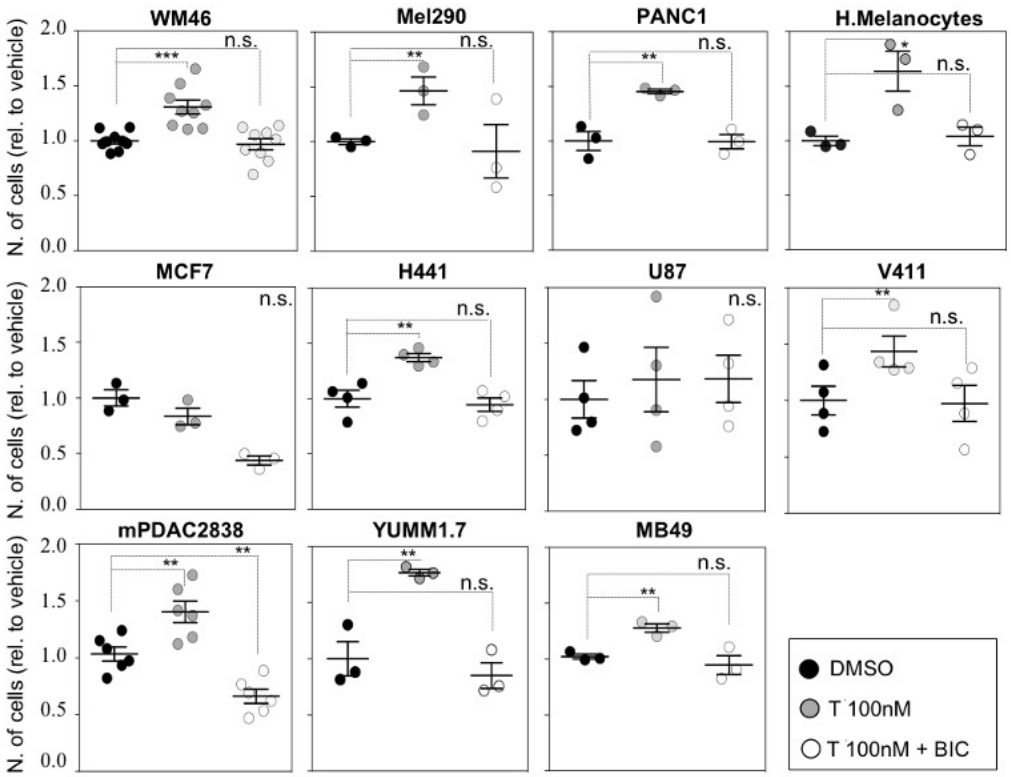

Cell types

WM46: Human skin melanoma
Mel290: Human uveal melanoma
YUMMS1.7: Murine skin melanoma
PANC1: Human pancreatic adenocarcionma
mPDAC: Murine pancreatic adenocarcinoma
MCF7: Human breast cancer
MB49: Mouse bladder cancer
H441: Human lung adenocarcionma
U87: Human glioblastoma
V411: Human adult acute myeloid leukemia

Fig. S8. Relative cell proliferation of a battery of cell lines derived from diverse tumor types in response to 100nM testosterone +/- bicalutamide treatment (2μM). *** p value≤0.001; ** p value≤0.01; * p value≤0.05; n.s>0.05.